OH formation by HONO photolysis during the BERLIOZ experiment

B. Alicke,[1] A. Geyer,[1,3] A. Hofzumahaus,[2] F. Holland,[2] S. Konrad,[2] H. W. Pätz,[2] J. Schäfer,[2] J. Stutz,[1,3] A. Volz-Thomas,[2] and U. Platt[1]

Received 2 March 2001; revised 17 July 2001; accepted 22 October 2001; published 15 January 2003.

[1] The photolysis of nitrous acid (HONO) in the early morning hours is an important source of OH radicals, the most important daytime oxidizing species. Although the importance of this mechanism has been recognized for many years, no accurate quantification of this OH source is available, and the role of HONO photolysis is often underestimated. We present measurements of HONO and its precursor NO_2 by Differential Optical Absorption Spectroscopy (DOAS) during the Berliner Ozonexperiment (BERLIOZ) field campaign in July/August 1998 at Pabstthum near Berlin, Germany. HONO concentrations, formation rates, and simultaneously measured HONO photolysis frequencies are used to calculate the total amount of OH formed by HONO photolysis during a full diurnal cycle. A comparison with the OH formation by photolysis of O_3 and HCHO and by the reaction of alkenes with ozone shows that HONO photolysis contributed up to 20% of the total OH formed in a 24 hour period during this campaign. In the morning hours, HONO photolysis was by far the most important OH source during BERLIOZ. *INDEX TERMS:* 0365 Atmospheric Composition and Structure: Troposphere—composition and chemistry; 0345 Atmospheric Composition and Structure: Pollution—urban and regional (0305); 0394 Atmospheric Composition and Structure: Instruments and techniques; *KEYWORDS:* HONO, photochemistry, OH, photolysis, HCHO, ozone

Citation: Alicke, B., A. Geyer, A. Hofzumahaus, F. Holland, S. Konrad, H. W. Pätz, J. Schäfer, J. Stutz, A. Volz-Thomas, and U. Platt, OH formation by HONO photolysis during the BERLIOZ experiment, *J. Geophys. Res.*, *108*(D4), 8247, doi:10.1029/2001JD000579, 2003.

1. Introduction

[2] The photolysis of nitrous acid (HONO) has been recognized as a potentially important production mechanism of OH radicals in the polluted urban atmosphere more than two decades ago [*Calvert et al.*, 1994; *Harris et al.*, 1982; *Jenkin et al.*, 1988; *Platt*, 1986; *Platt and Perner*, 1980]. Upon irradiation with light in the wavelength range from 300 to 405 nm, HONO decomposes forming an OH radical and NO (limiting the HONO lifetime typically to 10 min at noon) [e.g., *Stockwell and Calvert*, 1978; *Stutz et al.*, 2000]:

$$\mathrm{HONO} + h\nu \rightarrow \mathrm{OH} + \mathrm{NO} \quad (300\ \mathrm{nm} < \lambda < 405\ \mathrm{nm}) \qquad (1)$$

[3] The OH radical is by far the most important oxidizing species in the daytime atmosphere (see review by *Crutzen and Zimmermann* [1991]) in both polluted and clean areas. The quantification of OH formation mechanisms is therefore essential for the understanding of tropospheric chemistry and the ozone budget.

[4] On a global scale, the most important OH production mechanism is most likely the formation of excited $O(^1D)$ atoms from the photolysis of O_3 at wavelengths below 320 nm (reaction (2)) [e.g., *Logan et al.*, 1981]. The $O(^1D)$ atoms can react with water vapor to produce OH radicals directly (3) or be quenched by air molecules (4).

$$O_3 + h\nu \rightarrow O(^1D) + O_2 \quad (\lambda < 320\ \mathrm{nm}) \qquad (2)$$

$$O(^1D) + H_2O \rightarrow 2\ \mathrm{OH} \qquad (3)$$

$$O(^1D) + M \rightarrow O(^3P) + M \quad M = (N_2 \text{ or } O_2) \qquad (4)$$

[5] The branching ratio of reactions (3) and (4) (typically of the order of 10%) depends on the concentration of H_2O in ambient air and therefore also on the temperature (see section 3.5.2).

[6] A second source for OH is the photolysis of formaldehyde at wavelengths below 370 nm followed by rapid reaction of HO_2 with NO [*Meller and Moortgart*, 2000]:

$$\mathrm{HCHO} + h\nu \rightarrow \mathrm{H} + \mathrm{HCO} \quad J(\mathrm{HCHO_{rad}})(\lambda < 370\ \mathrm{nm}) \qquad (5)$$

$$\rightarrow H_2 + \mathrm{CO} \quad J(\mathrm{HCHO_{mol}}) \qquad (6)$$

$$\mathrm{H} + O_2 \rightarrow HO_2 \qquad (7)$$

$$\mathrm{HCO} + O_2 \rightarrow HO_2 + \mathrm{CO} \qquad (8)$$

$$HO_2 + \mathrm{NO} \rightarrow \mathrm{OH} + NO_2 \qquad (9)$$

[1]Institut für Umweltphysik, Universitat Heidelberg, Heidelberg, Germany.
[2]Stettiner Staatsforst, Forschungszentrum Jülich, Jülich, Germany.
[3]Department of Atmospheric Sciences, University of California, Los Angeles, Los Angeles, California, USA.

0148-0227/03/2001JD000579

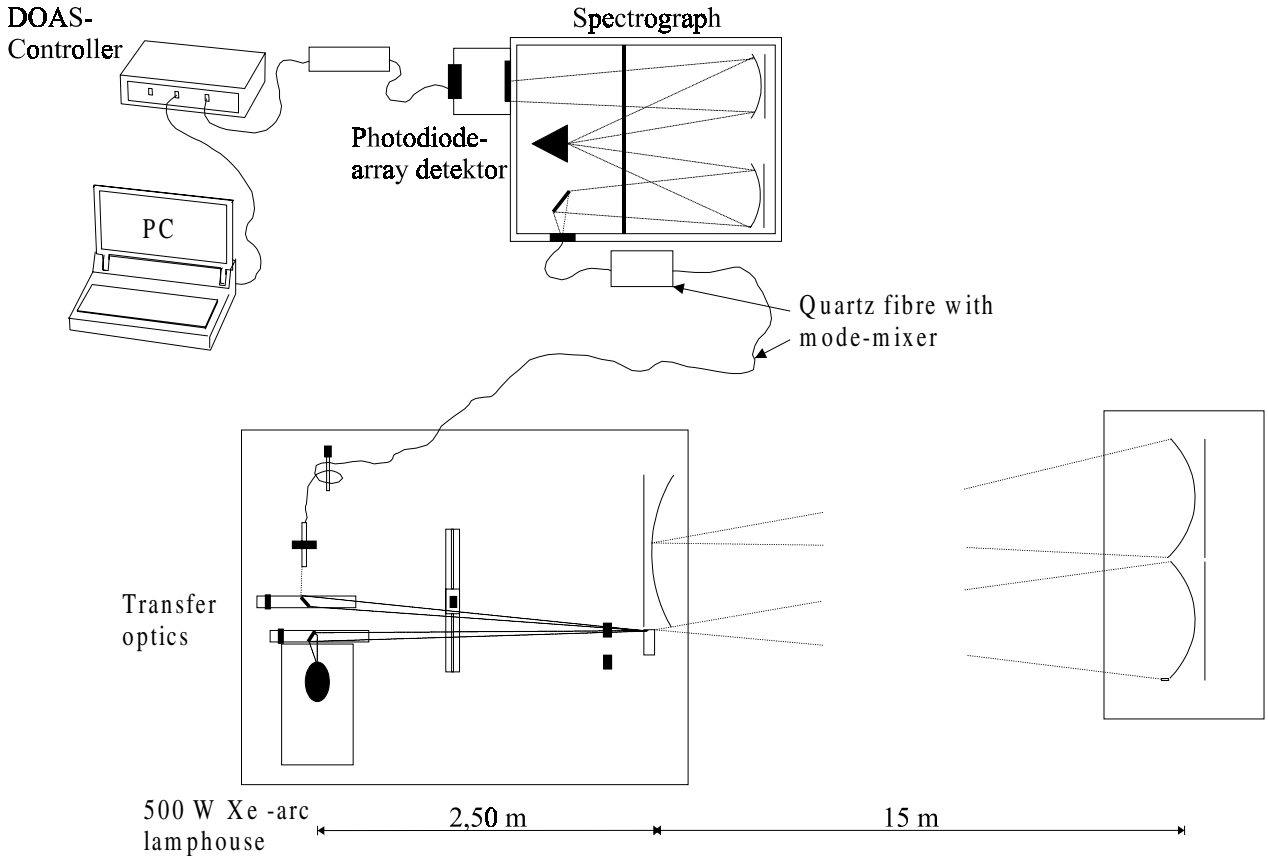

Figure 1. Schematic view of the setup of the DOAS White System used during the BERLIOZ campaign.

[7] The reactions of ozone with alkenes also lead to the production of OH radicals [*Atkinson and Aschmann*, 1993; *Paulson et al.*, 1997]. Ozone adds across the double bond to form a primary ozonide, which is not stable and decomposes to form a Criegee intermediate [*Criegee*, 1975]. This intermediate can either be stabilized or decomposed in a variety of ways (for a recent discussion refer to *Finlayson-Pitts and Pitts* [2000] and *Paulson et al.* [1999]). Therefore the alkene–ozone reaction represents a direct source of hydroxyl and peroxy radicals (OH + RO_2). The OH production yields of these reactions vary from 7% to 100% depending on the structure and size of the alkene [*Paulson et al.*, 1999].

[8] The reaction of RO_2 with NO represents another net source of OH radicals, if the RO_2 is not produced from OH reactions with hydrocarbons, but rather by ozonolysis of alkenes, or during the night by reactions of NO_3 with monoterpenes and other alkenes [*Bey et al.*, 2001; *Geyer et al.*, 2001, 2003; *Platt et al.*, 1990]. For a detailed discussion of the nighttime sources of OH during Berliner Ozonexperiment (BERLIOZ), see the work of *Geyer et al.* [2003].

[9] The contributions of the different mechanisms depend on the composition of the atmosphere. In remote regions with low NO_x and VOC concentrations, the photolysis of O_3 is probably the dominant source of OH. The importance of HCHO and HONO photolysis increases with the degree of pollution, e.g., increasing NO_x and VOC concentrations. The role of the ozone + alkene reactions depends on the presence of larger chain ($\geq$C5) alkenes, for example biogenic VOCs.

[10] The importance of the mechanisms also depends on solar radiation, and therefore the time of day. Due to their lower dissociation energy thresholds, the photolysis of HCHO and HONO starts earlier in the morning than that of O_3 (as far as the $O(^1D)$-forming channel is concerned). In contrast to HCHO, which levels are generally high throughout the day, the HONO concentrations often reach a maximum before or at sunrise. The photolytic lifetime of HONO is, however, roughly 2 orders of magnitude shorter than that of HCHO resulting in generally low HONO levels during day. The combination of elevated HONO concentrations at sunrise and the fast photolysis can therefore (in polluted areas) result in a peak production of OH surpassing all other sources in the morning. Over the day a steady state of HONO is generally established, and the importance of HONO as an OH source has often decreased.

[11] In contrast to the above mechanisms, the reactions of ozone and NO_3 with alkenes do not require sunlight. They therefore also proceed during the night (in the case of NO_3 almost exclusively at night) at a rate only depending

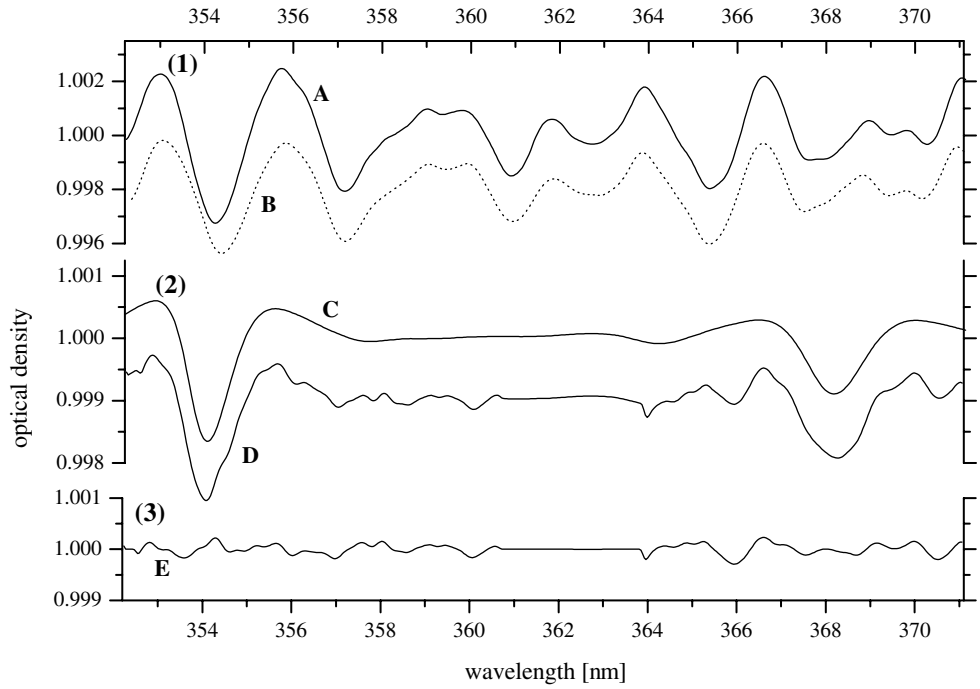

Figure 2. Example spectra for HONO and NO_2 analysis with the DOAS White system in Pabstthum. (1) Line A shows the atmospheric spectra, B is a NO_2 reference spectrum, which is the main absorber. (2) The residual after fitting all trace gases (except of HONO) to the atmospheric spectrum clearly shows the absorption structure of HONO (D, C is a HONO reference spectrum) with a concentration of 1.0 ± 0.09 ppb. (3) The residual structure of $\approx 10^{-4}$ (1σ) after simultaneous fitting of all trace gases (E).

on the ozone (or NO_3) and alkene concentrations. In polluted areas with high nighttime NO emissions near the ground, ozone (and NO_3) concentrations during the night and in the early morning are often low. In this case nighttime OH formation mechanisms are inefficient. But after the breakup of the nocturnal inversion and the dilution of the NO and entrainment from ozone aloft ozonolysis can become a significant OH source. In the time between sunrise and the beginning of vertical mixing, however, the photolysis of HCHO and, in particular HONO, frequently are the only OH sources.

[12] The first identification of HONO in the atmosphere was made by *Perner and Platt* [1979] and *Platt et al.* [1980]. Since then many atmospheric measurements have been reported [see *Lammel and Cape*, 1996; *Calvert et al.*, 1994 for reviews], with maximum mixing ratios of up to 15 ppb [*Winer and Biermann*, 1994] in Los Angeles or 10 ppb in Milan, Italy [*Febo et al.*, 1996]. Generally, HONO concentrations were found to scale with NO_2 concentrations, and therefore with the degree of pollution. The diurnal variation of the mixing ratio of HONO is dominated by its photolysis. During the night the concentration increases, showing a maximum before sunrise. The fast photolysis during sunrise is followed by a period of low concentrations during the day.

[13] Several studies have investigated the importance of HONO photolysis as an OH source, and its influence on ozone formation. The calculations are mostly based on assumptions about the formation of HONO. *Harris et al.* [1982] and *Sjödin* [1988] estimated OH production rates in the range of $(0.1-3) \times 10^7$ mol cm^{-3} s^{-1} for up to 8 ppb of HONO (measurement in Los Angeles) in the morning hours. A model study by *Harris et al.* [1982] found an increase of the maximum ozone concentration of up to 55% if 10 ppb of HONO are included (Los Angeles case, initial NO_x: 0.24 ppm). Another study [*Jenkin et al.*, 1988] found that the photolysis of HONO in the early morning results in a fivefold increase of OH at 0600 GMT, a 14% increase in OH present at the daily maximum (noon) and a 16% increase in net photochemical ozone production. Both studies agree that the increase of ozone starts much earlier due to the HONO photolysis in the morning.

[14] In order to quantify the importance of HONO as a precursor of the OH radical, its sources and sinks must be well investigated. HONO is known to be produced by reaction (10) [*Nguyen et al.*, 1998; *Stuhl and Niki*, 1972], but as this reaction removes OH, subsequent photolysis does not represent a net source of OH radicals.

$$OH + NO(+M) \rightarrow HONO(+M) \quad (10)$$

[15] It is long known that the bulk of urban HONO is formed via other pathways [e.g., *Platt*, 1986]. Production of HONO from the mechanisms summarized in reactions (11) or (12) involves only NO_x and water vapor. The photolysis of the HONO formed in (11) and (12) therefore represents a net source of OH radicals.

$$NO_2 + NO + H_2O \rightarrow 2HONO \quad (11)$$

$$2NO_2 + H_2O \rightarrow HONO + HNO_3 \quad (12)$$

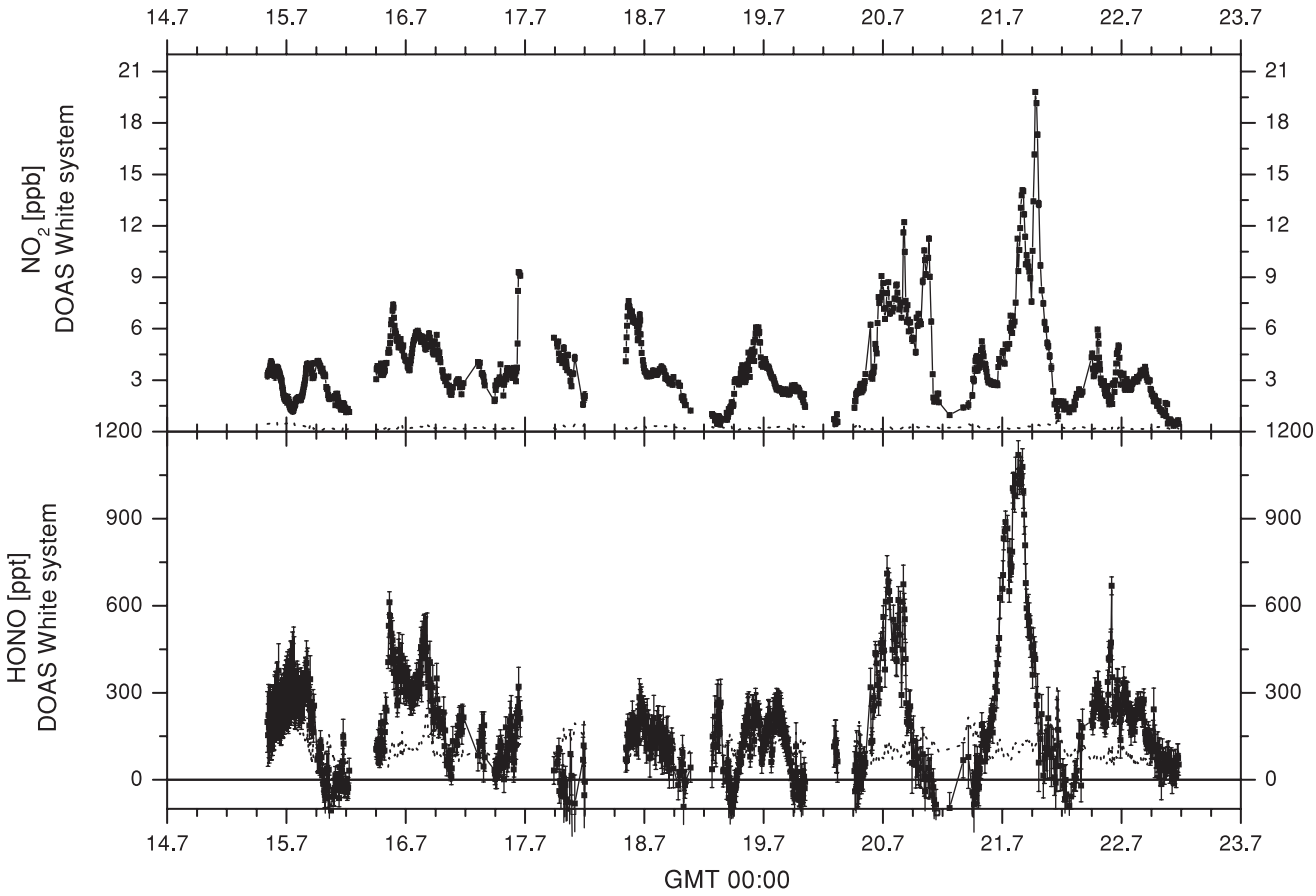

Figure 3. Time series of HONO and NO_2 measured by the DOAS White system. The diurnal variation as well as the correlation of both gases can be clearly seen. All error bars refer to the 1σ error calculated according to the work of *Stutz and Platt* [1996]. The dotted lines show the 2σ detection limits.

[16] These reactions seem to proceed heterogeneously on surfaces [*Ammann et al.*, 1998; *Goodman et al.*, 1999; *Junkermann and Ibusuki*, 1992; *Kalberer et al.*, 1999; *Lammel and Perner*, 1988; *Longfellow et al.*, 1998; *Notholt et al.*, 1992]. A number of laboratory studies [*Jenkin et al.*, 1988; *Pitts et al.*, 1984; *Sakamaki et al.*, 1983; *Svensson et al.*, 1987] have suggested that reaction (11) is not significant. Several field observations, where the presence of high ozone at night excluded NO or low NO was documented [*Harrison and Kitto*, 1994; *Kessler and Platt*, 1984], confirmed the laboratory results. Reaction (11) may become significant only in polluted air masses where the NO concentration is large. The exact mechanism of the heterogeneous formation of HONO summarized in reaction (12) is unknown, but several studies [e.g., *Jenkin et al.*, 1988; *Svensson et al.*, 1987] have shown that it is first order in NO_2 and water. The reaction rate seems to depend also on the type of surface.

[17] Other paths producing HONO like the reaction of NO_2 with HO_2 have been reported to be of minor importance [*Howard*, 1977; *Tyndall et al.*, 1995].

[18] The most important removal processes for HONO is its photolysis (1). A few percent of HONO is expected to be destroyed by OH radicals:

$$OH + HONO \rightarrow H_2O + NO_2 \quad (13)$$

[19] The self-reaction of HONO (14) [*Chan et al.*, 1976] and the reaction of HONO with nitric acid (15) [*Kaiser and Wu*, 1977] on surfaces might be important sinks in the nocturnal atmosphere.

$$2\ HONO \rightarrow NO + NO_2 + H_2O \quad (14)$$

$$HONO + HNO_3 \rightarrow 2\ NO_2 + H_2O \quad (15)$$

[20] The quantification of the OH production by HONO photolysis in the morning requires fast and precise measurement of HONO, especially during sunrise. Most measurements were so far performed with instruments of 0.5–12 hour time resolution [*Febo et al.*, 1993; *Harrison et al.*, 1996; *Sjödin and Ferm*, 1985], which is too slow to follow the decrease of HONO at sunrise. The recent improvement of Differential Optical Absorption Spectroscopy (DOAS) in our laboratory has increased the time resolution to 3–5 min, fast enough to determine the OH production at sunrise.

[21] Here we present high time resolution measurements of HONO, its precursor NO_2, and the HONO photolysis frequency during the Berliner Ozonexperiment 1998 (BERLIOZ). During the campaign other OH precursors like O_3, HCHO and alkenes were also measured as well as the photolysis frequencies and the ambient OH concentration. A quantitative comparison shows the diurnal variation, and

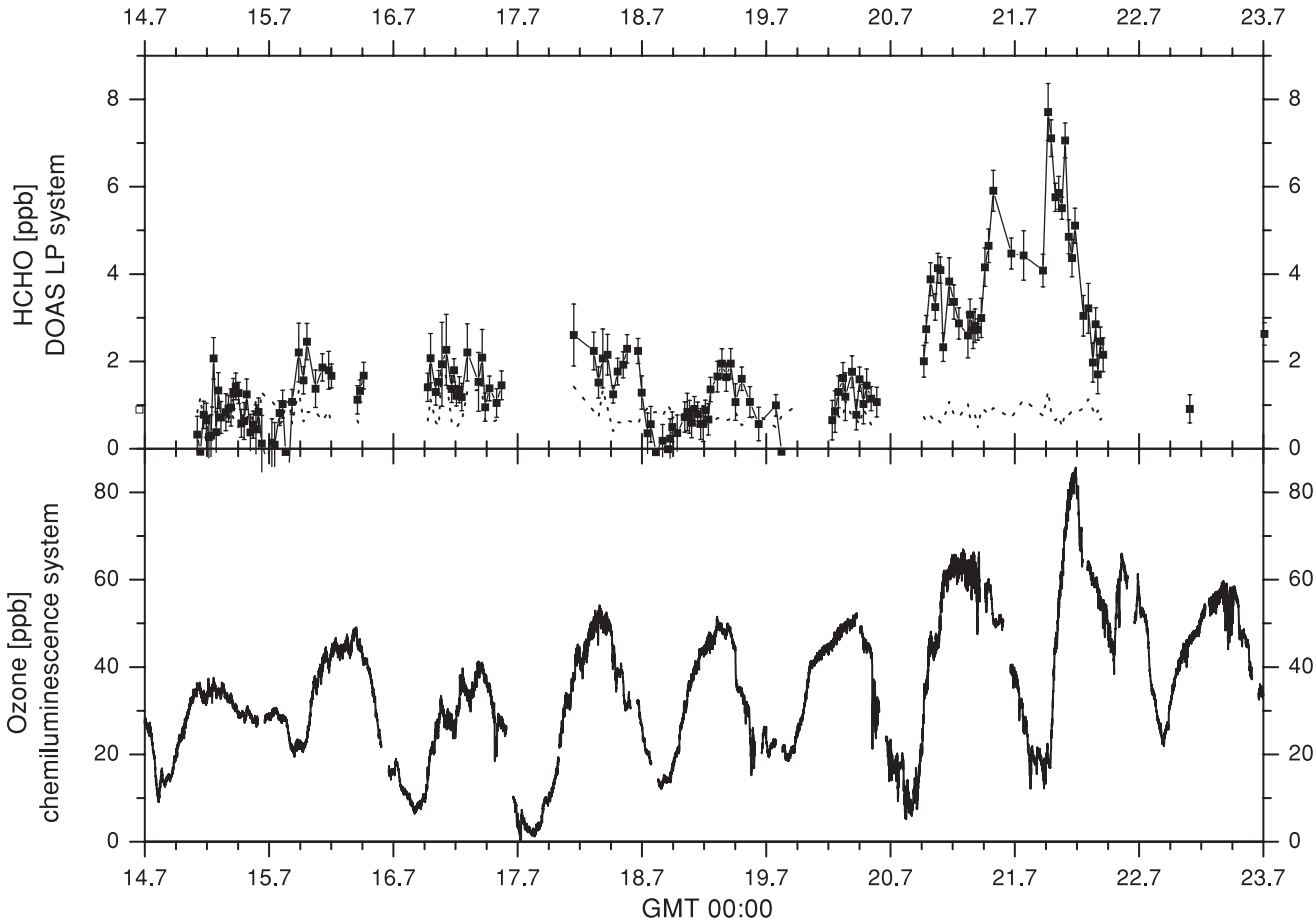

Figure 4. Time series of HCHO (DOAS LP system) and O_3 (in situ monitor). The dotted line refers to the 2σ detection limit for formaldehyde.

the relative importance of the HONO photolysis and the other OH production pathways.

2. Experimental Methods

2.1. Location

[22] The measurements were performed during the BERLIOZ from 12 July to 6 August 1998 [*Volz-Thomas et al.*, 2003a]. The station was located at the edge of a 7.5 × 4.5 km^2 flat meadow in the vicinity of the small village Pabsthum (12°56′25″ E, 52°51′15″ N, height: 50 m above sea level). This rural site has only little traffic and local anthropogenic emissions are therefore very small. The metropolis Berlin is situated in SE direction (145°) in a distance of 50 km (center) and 35 km (suburbs), respectively. The city of Neuruppin is located in the NW direction (12 km). A highway passes 14 km to the south of the site. The light path of a DOAS long path system pointed in an easterly direction from a height of 1.5 m at the site to the reflector at a distance of 2.5 km and 3.5 m above the ground. A DOAS White system together with the rest of the scientific instruments was mounted on a platform 8 m above ground.

2.2. Analytical Instruments

[23] A number of different instruments were operated at the station. Here only the DOAS instruments shall be discussed in detail. More details on the other instruments can be found in further publications in this issue.

2.2.1. In Situ Monitors for NO_2 and O_3

[24] Ozone was measured with a commercial short path UV absorption instrument (Thermo Instruments, TE49) with a time resolution of 1 min and a detection limit of 1 ppb. NO and NO_2 were detected by a gas-phase chemiluminescence system with a photolytic NO_2/NO converter (Eco Physics CLD 770 AL ppt with photolytic converter PLC 770). The measurement frequency of this system was 1 min with a detection limit of 20 ppt. A detailed description of the in situ monitors is given by *Volz-Thomas et al.* [2003b].

2.2.2. Gas Chromatograph for VOCs

[25] The mixing ratios of more than 50 hydrocarbons (including 27 alkanes, 10 aromatic hydrocarbons, 12 alkenes, isoprene, α-pinene, and the total amount of monoterpenes) were determined by gas chromatography with two different GC systems (HP-GC 5890 and Airmotec HC1010). Measurement procedures and data evaluation techniques are described by *Mihelcic et al.* [2003] and *Konrad and Volz-Thomas* [2001].

2.2.3. Spectroradiometer for Photolysis Frequency Measurements

[26] The photolysis frequency of NO_2 was measured with a 4π filter-radiometer (Meteorology Consult, 4π sr J(NO_2) Radiometer Nr. 631/632). A spectroradiometer was used to

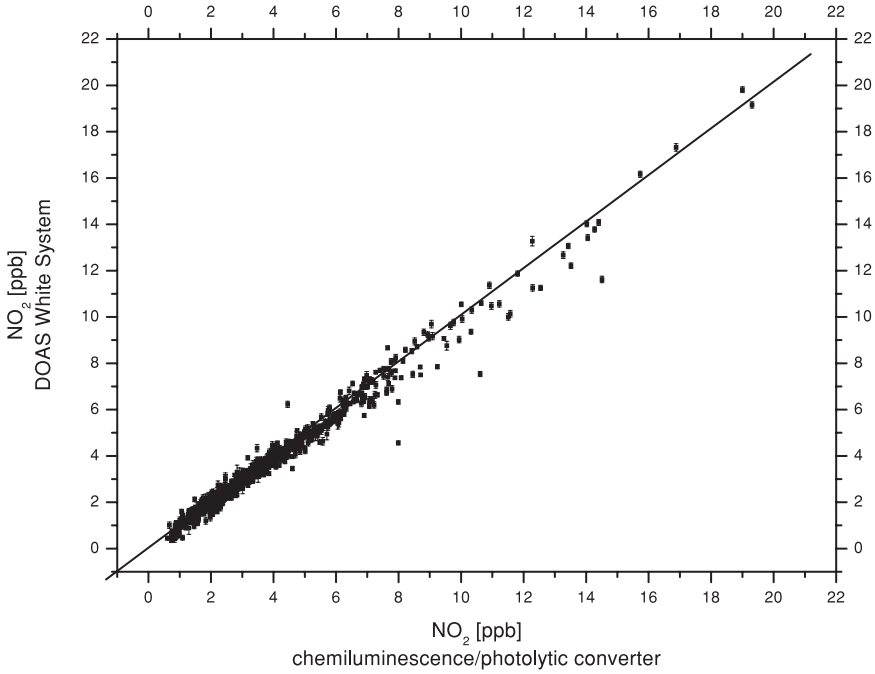

Figure 5. Intercomparison of the White system NO_2 data with that of the in situ monitor (Eco Physics CLD 770 ppt, Jülich). A linear regression analysis yields a good correlation of the two measurement techniques with a correlation coefficient of $R^2 = 0.98$. Because the error of the in situ monitor is about 7 times smaller, the regression was carried out by using only the errors of the White system.

measure the actinic flux (actinic flux spectroradiometer, Bentham DTM300) from which ozone and HCHO photolysis frequencies were calculated. These instruments are described in more detail by *Hofzumahaus et al.* [1999] and *Müller et al.* [1995].

2.2.4. Laser-Induced Fluorescence for OH and HO_2

[27] Laser-induced fluorescence (LIF) was used to determine the ambient concentration of OH and HO_2 during the *BERLIOZ* campaign. For a detailed description of the LIF measurement technique and evaluation algorithm for OH and HO_2 at *BERLIOZ*, refer to the works of *Holland et al.* [1998, 2003].

2.2.5. The DOAS Instruments

[28] DOAS is a technique that identifies and quantifies trace gases with narrow band absorption structures in the near UV and visible wavelength region in the open atmosphere. The fundamental setup of a DOAS instrument consists of a broadband light source, an optical system to transfer the light through the atmosphere, and a spectrograph-detector system to record the absorption spectra. These spectra show absorptions from different trace gases as well as extinction from air molecules and aerosol scattering. To extract the absorptions, and ultimately the concentration of the trace gases, DOAS separates the trace gas absorption cross section into two parts, one that varies slowly with wavelength, and a fast varying differential cross section σ'. Applying the same filtering procedure to the absorption spectrum leads to a differential absorption spectrum which can then be analyzed based on Lambert–Beer's law and σ'. For a detailed description of DOAS, see the review article by *Platt* [1994]. Two different DOAS systems were used at Pabstthum:

1. A DOAS long path (LP) system consisting of a single long light path, which is folded once between sending and receiving telescope. In short, the instrument consists of a double Newtonian sending and receiving telescope. The telescope collimates light of a Xe-arc lamp and sends it onto a quartz cube-corner retroreflector array, which reflects the beam back into the receiving telescope. The light is then fed through a quartz-fiber mode mixer [*Stutz and Platt*, 1997] into a spectrograph-detector system. The instrument measures trace gas concentrations averaged over the length of the light path. During BERLIOZ this system measured O_3, NO_2, HCHO, HONO, NO_3, and several aromatic hydrocarbons. Here we will concentrate on the formaldehyde measurements, which were made over a path of 2.5 km single length. A detailed description of the DOAS LP system is given by *Geyer et al.* [1999]. Note that it is possible that the DOAS LP system occasionally analyzed another air mass as the in situ instruments.

2. The concentrations of HONO and NO_2 presented here were measured with an open White type [*White*, 1942, 1976] f/100 multireflection system (see Figure 1) [*Ritz et al.*, 1992]. The base length of this DOAS White system was 15 m. Therefore, the system observed the same air mass as the in situ monitors, which were located within a few meters of the system. Absorption spectra were measured by alternatingly setting the cell to 16 and 144 traverses, leading to a total path length of 0.24 and 2.16 km, respectively. The White system was mounted inside an open heavy crane cantilever at a height of 8 m. No influence of the cantilever surface was expected since the residence time of the air inside the open cantilever structure was too short for any heterogeneous reactions to take place. Light of a Xe-arc lamp was fed into the system via a small Newtonian telescope. The spectrograph-detector system was coupled to the White system by another Newtonian telescope and a quartz fiber, which also performed the task of a mode mixer [*Stutz and Platt*, 1997].

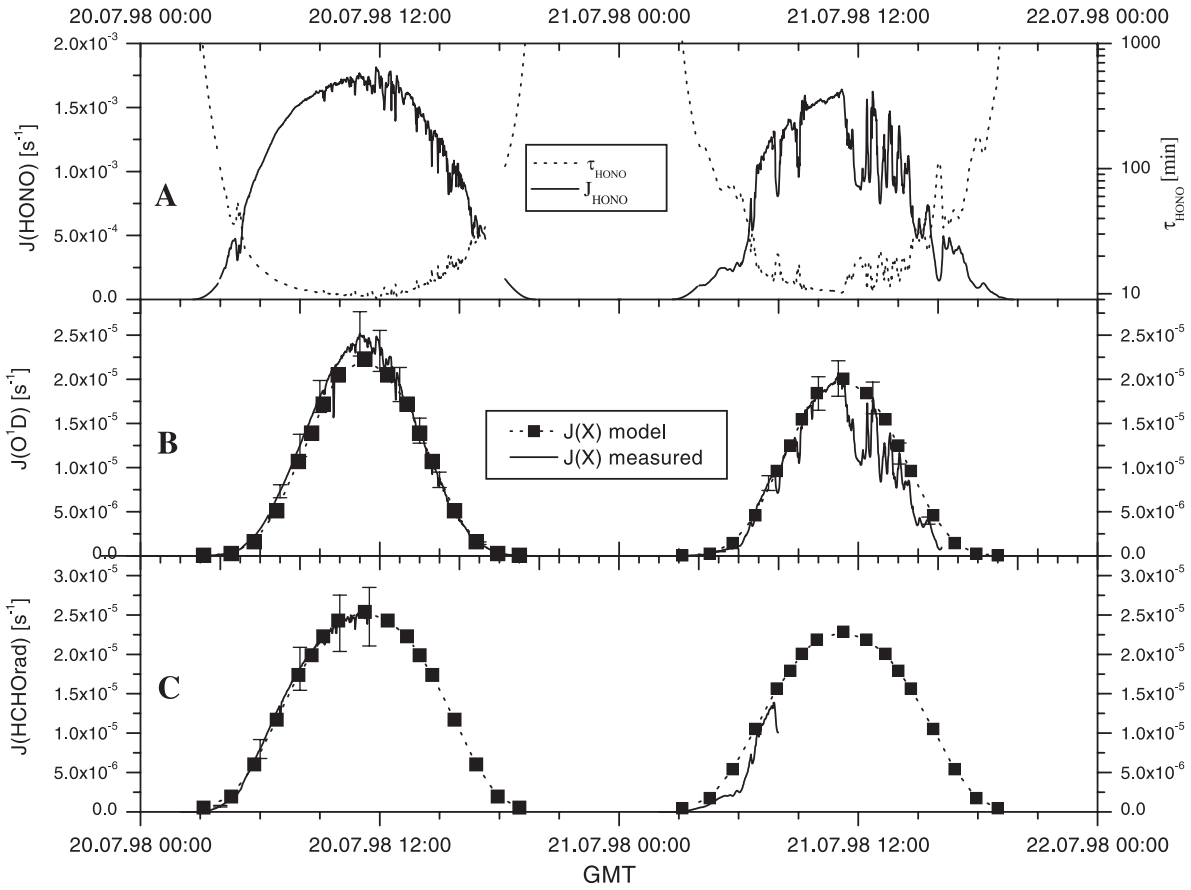

Figure 6. Comparison of the measured $J(HCHO_{rad})$ (graph C, see reaction (5)) and $J(O^1D)$ (graph B, reaction (2)) with the modeled values (squares) showing a good agreement within the uncertainty range. The measurement data for J(HCHO) have been available only until 1200 GMT on 20 July (0745 GMT on 21 July), but according to the good agreement it can be assumed that the model will match with the decrease in the afternoon as well. The average variance between model and measurement was 3.6% for the J(HCHO) model and 10% for the $J(O^1D)$, respectively. The measurement errors of $J(HCHO_{rad})$ = ±15% and $J(O^1D)$ = ±10% are included in the plot. In graph A, the photolysis frequency of HONO (left axis, solid line) and the corresponding lifetime of HONO due to photolysis (right axis, dotted line) are shown.

[29] Both DOAS systems used identical Czerny–Turner spectrographs with focal lengths of 0.5 m and photodiode array detectors [*Stutz and Platt*, 1992]. The spectrographs were held at a temperature of (+30 ± 0.3)°C. The detectors (HMT, Rauenberg) use a 1024 diode array (Hamamatsu S3904-1024N) of 25 μm center to center spacing and a height of 2.5 mm. The array was cooled by a Peltier element to (−30 ± 0.3)°C to reduce the dark current. The DOAS LP system used a 600 grooves mm^{-1} grating to measure a wavelength interval from 300 to 380 nm with a resolution of 0.54 nm. The DOAS White system observed a spectral interval from 337 to 377 nm, with a 1200 grooves mm^{-1} grating and 0.27 nm resolution. A UV band pass filter (UG5 Schott) in the light beam reduced stray light in the spectrograph.

2.3. Measurement Procedure and Analysis

2.3.1. The DOAS Long Path System

[30] The DOAS LP system measured different trace gases, taking alternating measurements on two (during the day) or three (at night) light paths. The time needed to change between the light paths and to automatically align the telescope determined the HCHO time resolution. Typically, a HCHO measurement was made every 30–90 min.

[31] The measurements employed the Multichannel Scanning Technique (MCST) [*Brauers et al.*, 1995; *Knoll et al.*, 1990; *Stutz*, 1996] to correct the diode to diode variation in the detector sensitivity. Additionally, spectra measuring scattered solar light and mercury wavelength standards were recorded frequently.

2.3.2. The DOAS White System

[32] Measurements of HONO and NO_2 were typically made every 5–20 min. Additionally to the spectra with 16 and 144 traverses spectra of the scattered light from the Sun and the light beams were recorded by blocking the lamp or one of the prisms respectively. All spectra were corrected for scattered sunlight, stray light and dark current. To correct the spectral characteristics of the lamp and the diode-to-diode sensitivity variations, the 144-path spectrum was divided by the 16-path spectrum.

2.3.3. Data Evaluation

[33] The spectra recorded by the two systems were analyzed with a combined linear/nonlinear least squares algorithm [*Stutz and Platt*, 1996], fitting trace gas reference spectra and a emission spectrum of the lamp, together with a polynomial of 8th order, to the atmospheric spectrum. The concentration of the respective trace gases can then be determined by the scaling parameters of the reference spectra and the differential absorption cross section. After all known absorbers are removed from the measured spectrum by subtracting their scaled reference spectra, a residual structure will remain, representing the electronic noise of the instrument and unknown absorbers. Figure 2 shows an example of such an evaluation of an atmospheric spectrum (line A) recorded with the White system. The remaining residual structure after subtracting the reference spectra is shown at the bottom (line E). To eliminate peak residual structures in the spectrum between 361 and 364 nm, a rectangular smoothing function was applied. Over the period of observation presented here the mean size of the residual structure was 0.5×10^{-3} (peak to peak) for the White system (1.4×10^{-3} for the LP system).

[34] The error of the concentration determined by the least squares fitting procedure underestimates the "true" statistical error and was therefore multiplied by a factor of 3 (all errors in this paper refer to the 1σ error) [*Stutz and Platt*, 1996]. During the BERLIOZ campaign, a mean detection limit of HCHO of 0.7 ppb was thus determined (we define the detection limit as twice the 1σ error). The detection limits for HONO and NO_2 were 84 ppt and 0.23 ppb respectively. The uncertainty of the formaldehyde cross section is ±5% [*Meller and Moortgart*, 2000], for HONO ±5% [*Stutz et al.*, 2000] and ±8% for the NO_2 cross section [*Schneider et al.*, 1987]. The systematic error of the DOAS spectrometer was determined by *Stutz* [1996] as <3%. The total systematic error of the HCHO, HONO, and NO_2 concentrations determined by DOAS are therefore <6%, <6%, and <9% respectively.

3. Results

3.1. Time Series of NO_2, HONO, O_3, and HCHO

[35] Figures 3 and 4 show the time series of the mixing ratios of NO_2, HONO, O_3 and HCHO. Nitrogen dioxide levels varied from values near the average detection limit of 0.24 ± 0.1 ppb of the White System to a maximum of 20.4 ± 0.4 ppb in the early morning hours (0640 GMT) of 21 July 1998. The high NO_2 concentrations on this and the following day can be explained by southerly winds transporting polluted air from Berlin to the station, as indicated by trajectory analysis. The ozone concentration varied from the detection limit of 1–85.2 ppb during 21 July. Similarly, HCHO reached its maximum of 7.7 ppb in the morning of 21 July 1998. It should be noted that the formaldehyde measurements carried out at a height of 8 m with a Hantzsch monitor [see *Grossmann et al.*, 2003] yielded roughly two times smaller values. The cause of this discrepancy could not be resolved yet and is discussed by *Grossmann et al.* [2003]. HONO mixing ratios were below 500 ppt throughout the beginning of the campaign. The HONO daytime values never exceeded the average daytime detection limit of 0.11 ± 0.05 ppb (except for the early morning hours).

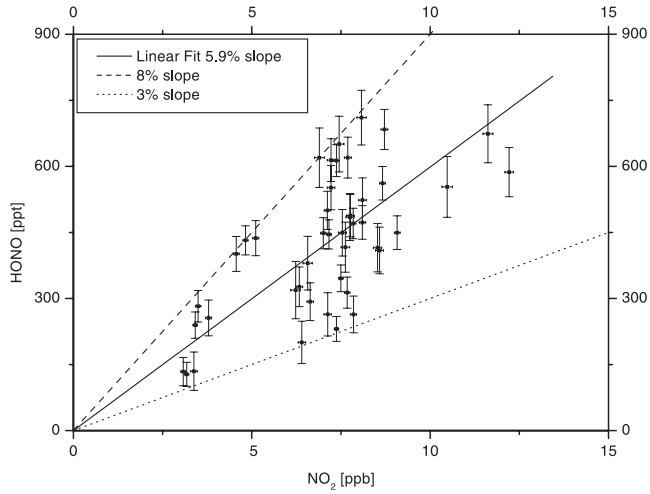

Figure 7. Correlation of HONO to NO_2 for the night 19/20 July 1998. An average slope of 5.9% (3–8%) can be derived from the data.

Higher levels were observed during the nights of 19/20 and 20/21 July 1998, when also the NO_2 levels were highest (see Figure 3). HONO shows the typical diurnal cycle with increasing concentrations during the night, reaching the highest values shortly before sunrise (e.g., 1.11 ± 0.05 ppb at 0315 GMT on the 21 July).

[36] In the following we will concentrate on the period from the evening of 19 July to the evening of 21 July 1998, the days with the highest photochemical activity and ozone formation rates.

3.2. Intercomparison of the NO_2 Measurements

[37] To control the performance of the two NO_2 instruments at Pabstthum an intercomparison of the DOAS and the chemiluminescence/photolytic-converter system data was made. Due to the different measurement intervals, the more frequent NO_2 chemiluminescence data were integrated over the longer measurement interval of the DOAS White system. A total of 1043 simultaneous data points were calculated by this method (Figure 5). A linear regression weighted by the error of the DOAS system yields a slope of 1.006 ± 0.005 (White system against chemiluminescence system) and a statistically insignificant intercept of 36 ± 19 ppt (see Figure 5). The square of the correlation coefficient was $R^2 = 0.98$. The error of the regression is dominated by the random error of the DOAS data, which is about 6 times higher compared to the uncertainty of the in situ monitor (typically 20 ppt).

[38] This agreement is surprisingly good considering that the systematic error of the DOAS data, which is mainly determined by the uncertainty of the literature cross section [*Schneider et al.*, 1987], is about 9%. The excellent agreement between the DOAS system and the in situ monitor suggest that either the cross section by *Schneider et al.* [1987] is more precise than the uncertainty suggests, or that by coincidence the systematic errors of the systems cancel each other. Nevertheless, the comparison demonstrates the high reliability and quality of the NO_2 data obtained by both systems.

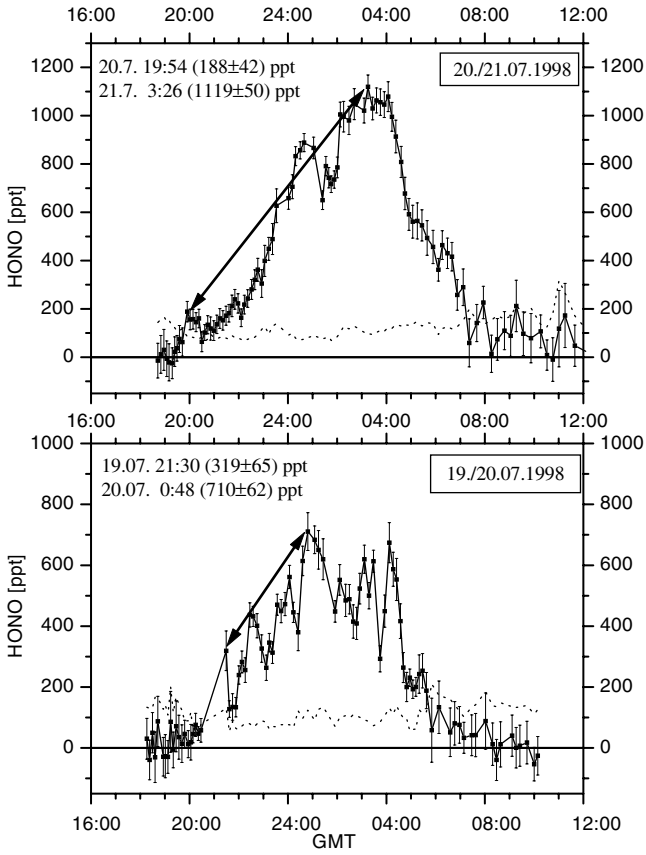

Figure 8. The increase of HONO during the nights 19/20 and 20/21 July 1998. The arrows mark the slopes used for the calculation of the HONO production rates (reaction (17)). HONO accumulates during the night until a maximum value is reached latest when the photolysis of HONO starts. During the increase of HONO, the NO_2 concentration has been relatively constant on 20 July but was increasing as well on 21 July. The dotted lines refer to the 2σ detection limits.

3.3. Intercomparison of Modeled Photolysis Frequencies With Measurements

[39] Figure 6 shows the photolysis frequencies of ozone, HCHO and HONO measured during the campaign. The photolysis frequency of HONO was obtained using the measured $J(NO_2)$ following the approach by *Kraus and Hofzumahaus* [1998] (The accuracy of the measured $J(NO_2)$ is ±7%):

$$J(HONO) = 0.189 \cdot J(NO_2) + 8.433 \cdot 10^{-2} \cdot [J(NO_2)]^2 \quad (16)$$

[40] From the data it can be seen that the morning of 20 July was clear, resulting in smooth photolysis curves. In the afternoon of the same day the effect of some clouds is apparent. 21 July showed a stronger short-term variability in the photolysis data. Especially after noon, the photolysis frequency drops by 30% for about 1 hour. The data of the photolysis frequency for HCHO has some considerable gaps in this 2 day period. To fill in gaps in the photolysis data we applied a radiative transfer model [*Ruggaber et al.*, 1994] for sunny and cloud-free days. The values for the vertical column of pressure, temperature, water vapor, aerosol distribution, NO_2, SO_2, and O_3 were taken for a typical summer day in the European midlatitudes. The ground was assumed to be isotropic, consisting mainly of grass with rocks (asphalt) [Albedo: 0–0.65 depending on the wavelength region (280–4000 nm)]. To validate the model, an intercomparison between the measured values of J(HCHO) and $J(O^1D)$ was carried out (see Figure 6). The agreement between model and measurement is better than 96% for J(HCHO) and 90% for $J(O^1D)$ respectively. The uncertainty of the spectroradiometer is ±10% for $J(O^1D)$ and ±15% for J(HCHO). It should be noted that the HCHO photolysis frequencies modeled for clear day conditions slightly overestimate the actual photolysis frequencies.

3.4. The HONO Source Strength

[41] To derive the daytime HONO formation rate we will assume that HONO formation is independent of the actinic flux. In other words, the same NO_2 to HONO conversion processes occur day and night. We assume that the atmospheric formation of HONO proceeds exclusively via reaction mechanism (12). Our observations indicate that this conversion most likely takes place on the ground. Our results support this approach for the following reasons:

1. The reaction path including NO (11) was of minor importance because of the very low concentrations of NO during the night (a few 10 ppt in the maximum) [cf. *Geyer et al.*, 2001].

2. A correlation between the NO_2 to HONO conversion frequency and the aerosol surface was not found. Although, for example, the aerosol surface area (as measured by an optical particle counter; Pallas PCS2000) increased by a factor of 4.5 from the night of 19 July to the following night such an increase in the HONO formation was not observed. Recent gradient measurements in Milan, Italy, also proved that HONO is mostly formed on the ground [e.g., *Veitel*, 2002; *Stutz et al.*, 2002].

3. As pointed out by *Stutz et al.* [2002] one expects that HONO will reach a steady state when its formation and loss rates are equal: The main loss of HONO at night is deposition. If, as assumed here, HONO is formed by a first order conversion of NO_2 one expects a constant HONO/NO_2 ratio in this steady state. The HONO mixing ratios in the second half of the night during BERLIOZ followed the NO_2 levels (Figure 3), indicating that the steady state was indeed achieved. On an average the nighttime HONO/NO_2 ratios were between 3% and 8%. Figure 7 presents the correlation of HONO to NO_2 for the night of 19/20 July, when a mean ratio of 5.9% was calculated. A correlation of HONO and NO_2 with ratios around 2–10% was also observed in many other studies [e.g., *Alicke et al.*, 2002; *Allegrini and Febo*, 1995; *Febo et al.*, 1996; *Lammel and*

Table 1. Overview of the Integrated Morning and Daytime OH Production by HONO Photolysis

Day	$\int_{morning}$ OH dt (by HONO photolysis) [ppb]	NO_2 to HONO conversion rate [%/hr]	$\int_{daytime}$ OH dt (by HONO photolysis) [ppb]
20 July	1.0 ± 0.2	1.5 ± 0.5	0.8 ± 0.4
21 July	1.8 ± 0.25	2.1 ± 0.8	1.4 ± 0.5

The NO_2 to HONO conversion rate was derived from the data of the night before (see Figure 8 and text).

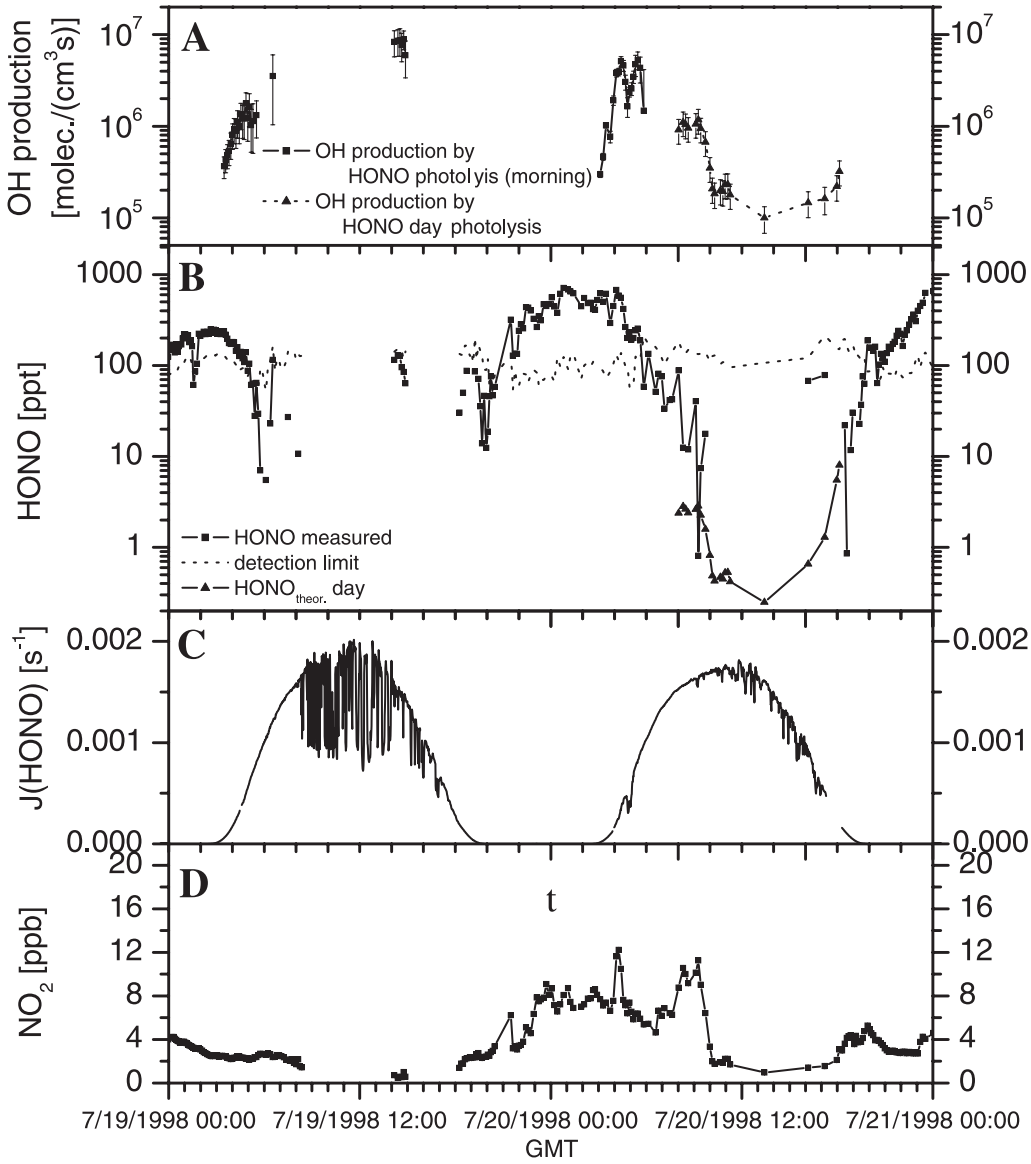

Figure 9. The measured HONO and NO_2 concentration from 19 to 21 July 1998. Graph A shows the OH production rate by HONO photolysis for the morning and the net daytime production of hydroxyl radicals (calculated with reaction (18), triangles). In graph B, the measured HONO concentrations (night and morning) as well as the calculated HONO concentrations during daytime (triangles, derived by the steady state assumption (19)) is printed. Graph C shows the measured HONO photolysis frequencies. The NO_2 concentration in graph D is measured with the DOAS White system.

Cape, 1996; *Platt*, 1986]. We therefore feel confident that the conversion of NO_2 on the ground is indeed the mechanism responsible for the formation of HONO during BERLIOZ.

[42] To estimate the strength of HONO formation by reaction (12) during the day we extrapolated this NO_2 to HONO conversion during the first half of the night to daytime conditions. Figure 8 shows that the HONO mixing ratio increases steadily after sunset and reaches a maximum sometime after midnight. Taking the individual nights, we determined the HONO formation by assuming a linear increase of its mixing ratio during a time interval ($t_2 - t_1$). Because of the conversion should be first order in NO_2, we scaled the HONO formation rate with the average NO_2 concentration. This largely compensates the dependences of the HONO concentration toward both its formation from NO_2 and its dilution by vertical mixing (Since both NO_2 and HONO are formed near the ground any transport process like vertical dilution will not alter the HONO/NO_2 ratio).

[43] The average nighttime HONO conversion frequency (HONO production rate scaled with the average NO_2 mixing ratio) was then determined for the nights of 19/20 and 20/21 July by:

$$\overline{C_{HONO,night}} = \frac{[HONO](t_2) - [HONO](t_1)}{(t_2 - t_1) \cdot \overline{[NO_2]}_{night}} \qquad (17)$$

Table 2. Comparison of the Different OH Production Rates During BERLIOZ

Day	Time [GMT]	Species X	J_x [s^{-1}]	[X] [ppb]	OH production rate [$\times 10^6$ cm^{-3} s^{-1}]
20 July	0520	HONO	$(8.4 \pm 0.6) \times 10^{-4}$	0.25 ± 0.05[a]	5.3 ± 1.1
		HCHO	$(4.1 \pm 0.7) \times 10^{-6}$	1.6 ± 0.5[a]	0.3 ± 0.2[a]
		O_3	$(1.4 \pm 0.1) \times 10^{-6}$	13 ± 1	0.1 ± 0.01
		$VOC + O_3$	see Table 3		0.3 ± 0.1
21 July	0700	HONO	$(8.4 \pm 0.6) \times 10^{-4}$	0.28 ± 0.08	8.0 ± 2.1
		HCHO	$(1.2 \pm 0.2) \times 10^{-5}$	7.1 ± 0.4	4.5 ± 0.7
		O_3	$(5.8 \pm 0.6) \times 10^{-6}$	21 ± 1	0.9 ± 0.1
		$VOC + O_3$	see Table 3		0.7 ± 0.3

[a]Estimated, no LP-DOAS HCHO data at 0520.

[44] The results of this calculation are shown in Figure 8 and Table 1. Assuming that HONO is formed during the day by the same mechanisms as during the night, the production rate at any time t can then be determined by:

$$P_{HONO,day}(t) = \overline{C_{HONO,night}} \cdot [NO_2](t) \quad (18)$$

[45] Regarding the steady state between OH, NO and HONO due to reactions (10) and (1), this additional HONO formation will lead to a net OH production rate during the day, with $P_{OH}(t) = P_{HONO,day}(t)$. The simultaneous measurements of NO, OH, J(HONO), and our estimation of the daytime production of HONO by reaction (18), makes it possible to estimate the steady state concentration of HONO during day. Figure 9 shows the daytime HONO concentrations calculated by a steady state approach using:

$$[HONO] = \frac{k_{(10)} \cdot [OH] \cdot [NO] + P_{HONO,day}}{J(HONO)} \quad (19)$$

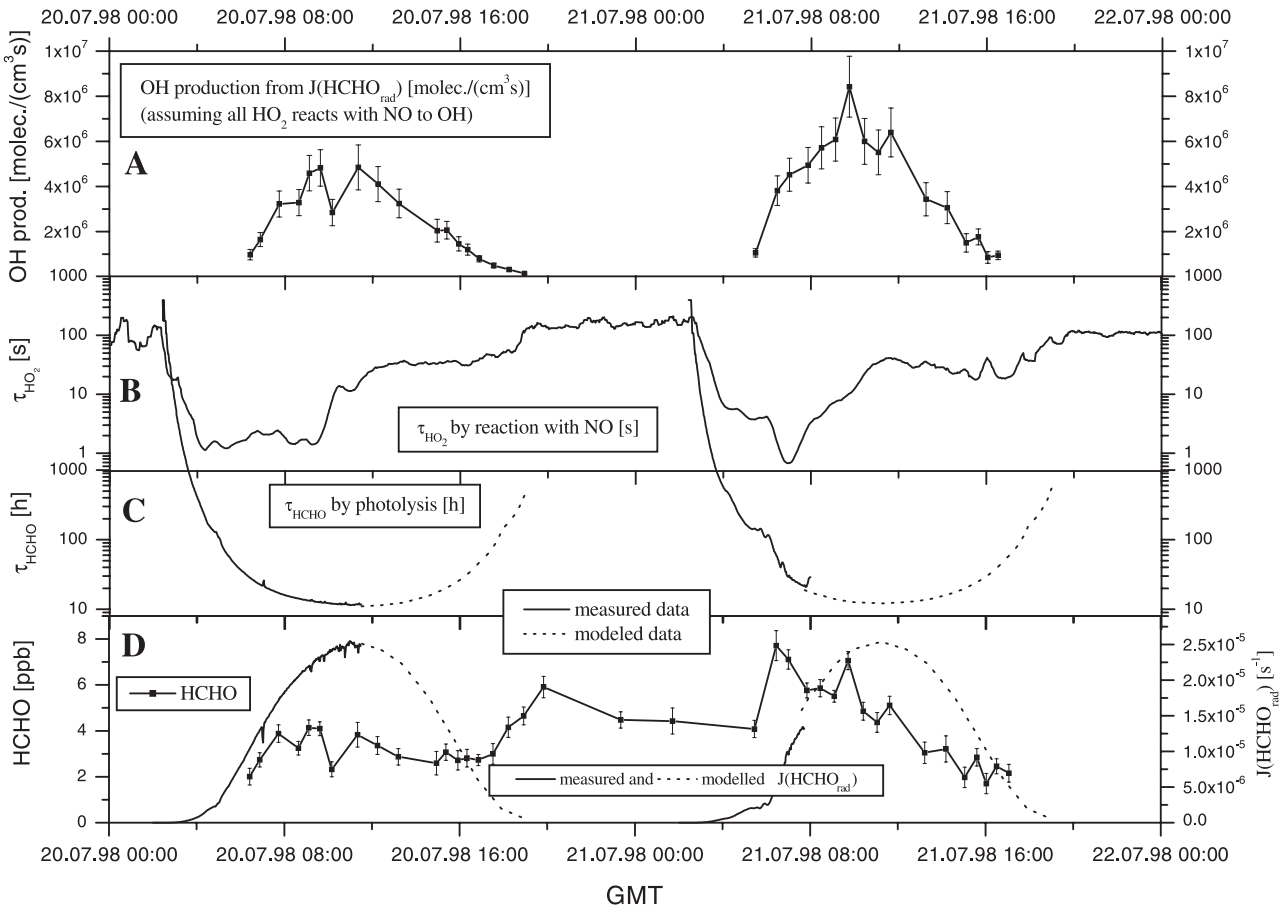

Figure 10. The lifetime of HO_2 due to the reaction with NO (see reaction (9)) (timescale seconds) and to photolysis (timescale hours) are shown in graphs B and C, respectively. The diurnal variation of HCHO can be seen in graph D (left axis) together with its photolysis frequency $J(HCHO_{rad})$ (right axis). Graph A shows the production of hydroxyl radicals by the photolysis of formaldehyde and the immediately reaction with NO afterward.

Table 3. Overview of the VOCs Used to Derive the OH Production by Ozonolysis During BERLIOZ Including Their Reaction Constants [*Atkinson*, 1997] and OH Formation Yields [*Paulson et al.*, 1999]

Species	$k_{O3} \times 10^{-18}$ [cm^3 s^{-1}]	OH formation yield[c]	Average[b] concentration [ppb]	Percent of each VOC on total VOC → OH production[b]
Ethene	1.59	0.18 ± 0.06	0.499	1.1
Propene	10.10	0.35 ± 0.07	0.122	3.7
i/1-Butene	9.64	0.29 ± 0.04	0.072	1.8
1,3-Butadiene	6.30	0.13 ± 0.03	0.014	0.1
trans-2-Butene	190.00	0.64	0.005	8.0
cis-2-Butene	125.00	0.37 ± 0.2	0.009	3.8
1-Pentene	10.00	0.24 ± 0.07	0.014	0.2
3-Methyl-1-Butene	11.00	0.24	0.006	0.1
2-Methyl-1-Butene	16.00	0.67 ± 0.12	0.029	1.3
Isoprene	12.80	0.13 ± 0.03	0.332	9.5
cis-2-Pentene	140.00	0.30	0.004	2.1
trans-2-Pentene	160.00	0.47	0.012	5.4
2-Methyl-2-butene	403.00	0.89 ± 0.4	0.007	18.0
Cyclopentene	570.00	0.61	0.000	0
1-Hexene	11.00	0.18 ± 0.05	0.005	0.1
cis-3-Hexene	150.00	0.36	0.012	4.1
cis-2-Hexene	150	0.33	0.002	1.3
trans-2-Hexene	170.00	0.40	0.010	6.9
Styrene	17.00	0.07	0.0001	0
α-Pinene	86.60	0.70 ± 0.17	0.166	29.5
β-Pinene[a]	15.00	0.35 ± 0.17	0.011	0.2
Δ3-Carene[a]	37.00	1.00 ± 0.45	0.013	1.4
Myrcene[a]	470.00	1.00 ± 0.45	0.0005	0.7
Camphene[a]	0.90	0.10 ± 0.05	0.050	0
γ-Terpene[a]	140	1	0.0001	0.1
Sabinene[a]	86.00	0.26 ± 0.11	0.002	0.1
β-Phellandrene[a]	47.00	0.14 ± 0.06	0.005	0.1
d-Limonene[a]	200	0.86 ± 0.4	0.0006	0.3

[a]Concentration calculated from the total amount of monoterpenes [see *Geyer et al.*, 2001].

[b]Average over the 20 and 21 July 1998.

[c]Partly no error for the OH formation yield could be found in literature.

[46] At noon the lowest mixing ratios of around 5 ppt were calculated (at this time NO_2 was typically around 1 ppb). These values are well below the detection limit of our instruments.

3.5. Quantification of the OH Production Rates

3.5.1. OH Production by HONO Photolysis

[47] The amount of OH formed by HONO photolysis was estimated in two parts. The first uses the available morning data of HONO and J(HONO). The second estimates the production rate of HONO from our nighttime measurements and extrapolates them to derive daytime OH production rates (as discussed above, reactions (17)–(19)). To derive the 24 hour integrated OH production these two terms were added.

[48] The time series of the OH production rates for the two selected days are shown in Figure 9. Starting at sunrise HONO is photolyzed into NO and OH and yields a peak in the early morning OH production rate. The maximum OH production rate during this period was $(8.0 \pm 2.1) \times 10^6$ cm^{-3} s^{-1} at 0700 GMT on 21 July. The different values for the 2 days discussed here are summarized in Tables 1 and 2.

3.5.2. OH Production by Ozone Photolysis

[49] To calculate the OH production rate by ozone photolysis we used relative humidity data and temperature to derive absolute water concentrations. Together with the measured O_3 concentration and the photolysis frequency the amount of OH produced according to reactions (2)(3)–(4) is calculated. The average fraction of $O(^1D)$ reacting with water to OH over the complete campaign was 10.3% with variations from 6 to almost 15%. The OH production rate by ozone photolysis was, as expected, highest during the highest UV radiation around noon and negligible during the night due to the lack of photolysis.

3.5.3. OH Production by HCHO Photolysis

[50] The OH production rate by the photolysis of formaldehyde was calculated assuming that the produced HO_2 by the reaction schemes (5), (7), and (8) is immediately converted into NO_2 by reaction (9). Figure 10B compares the lifetime of HO_2 for the NO concentrations observed during BERLIOZ. In the morning with concentrations of NO in the range of 1–9 ppb τ_{HO2} is 5–0.5 s. In the afternoon NO mixing ratios of about 0.2 ppb lead to an HO_2 lifetime of 25 s. The photolysis of formaldehyde with a lifetime of about 10 hours at noon (Figure 10) is much slower than the conversion of HO_2 to OH, which therefore was the rate-determining step for the production of OH radicals from HCHO photolysis. The OH production rate from HCHO photolysis followed closely the solar radiation and showed a maximum of $(8.4 \pm 1.4) \times 10^6$ cm^{-3} s^{-1} at 0945 GMT (see Figure 10).

3.5.4. OH Production of the Reaction of VOCs With Ozone

[51] The OH production rate from the reaction of ozone with alkenes, as recently reviewed by *Paulson et al.* [1999], was calculated by taking the OH formation yield of each reaction into account (see Table 3). Due to the rural site, high amounts of biogenic VOCs were present. Since only α-pinene was measured directly, we used the calculations published by *Geyer et al.* [2001] to estimate the concentrations of other monoterpenes. These calculations were based on emission factors of the surrounding vegetation. Table 3 also lists the rate constants of the reaction of the VOCs with O_3 and the yield of OH. Based on this data we calculated the formation of OH radicals from ozonolysis throughout the day. The last column in Table 3 shows the relative contribution of the individual VOCs from 19 to 21 July 1998, at Pabstthum. During BERLIOZ α-pinene and 2-methyl-2-butene were the most important compounds. Since our measurements and calculations did not consider all VOCs, which might be present, our calculation only represents a lower limit of this mechanism.

Table 4. Comparison of the Integrated OH Production Over 24 Hours for the 20/21 July 1998 at the BERLIOZ Site Pabstthum

Day	Species	Reaction scheme	Percent of total OH production	OH production in 24 hours [ppb]
20 July	O_3	(2) + (3)	45	6.0 ± 0.7
	HONO	(1)	14	1.9 ± 0.4
	HCHO	(5) + (7) − (9)	35	4.6 ± 0.9
	VOC + O_3	[a]	6	0.8 ± 0.3
	NO_3	[a]	<1	0.1 ± 0.05
21 July	O_3	(2) + (3)	32	5.2 ± 0.6
	HONO	(1)	20	3.2 ± 0.6
	HCHO	(5) + (7) − (9)	39	6.4 ± 1.2
	VOC + O_3	[a]	7	1.2 ± 0.5
	NO_3	[a]	<2	0.3 ± 0.15

[a]Several reactions.

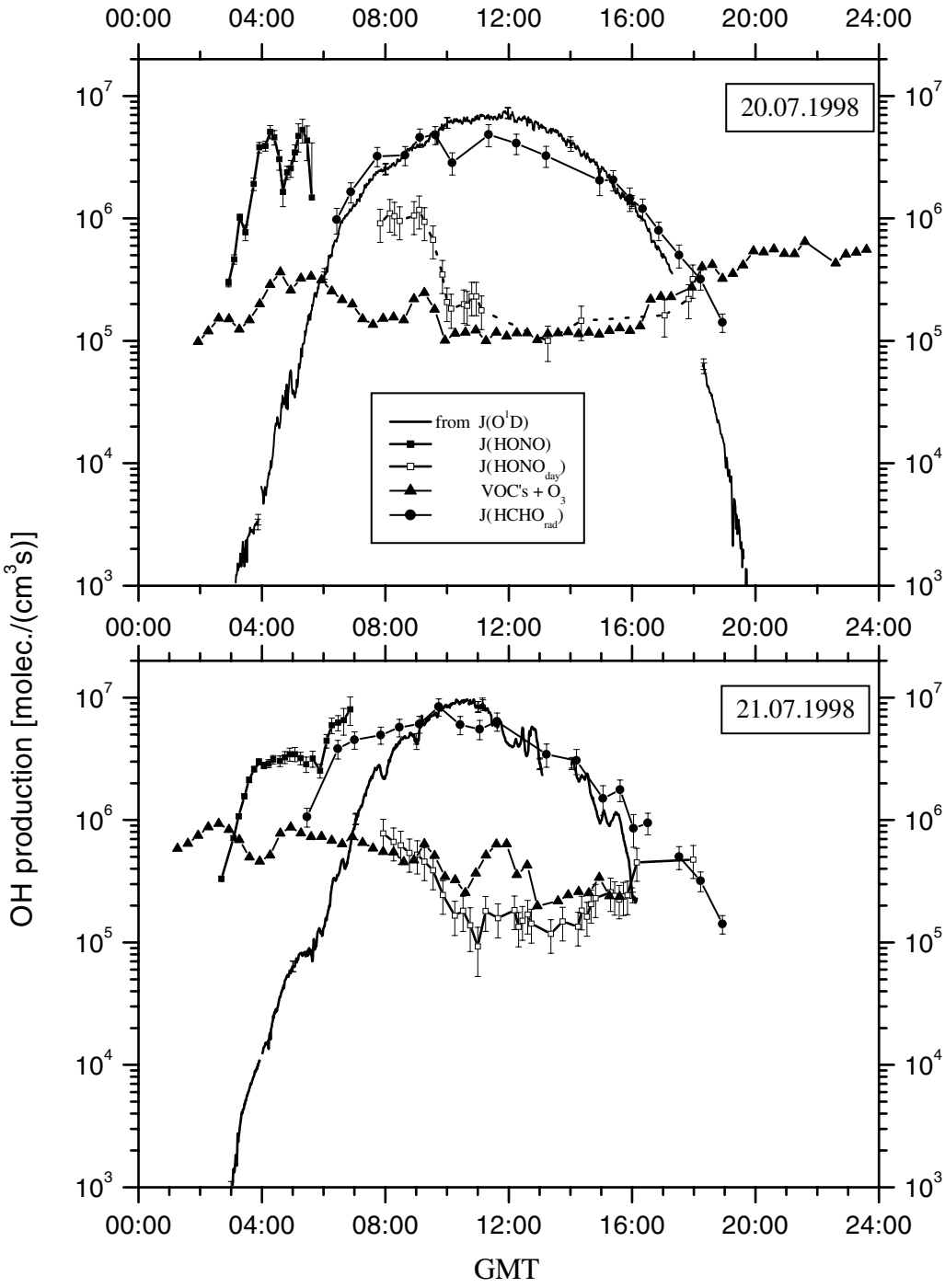

Figure 11. Comparison of the four main OH sources for the 20/21 July 1998 at the Pabstthum site of the BERLIOZ campaign. For a better overview, the data are plotted on a logarithmic scale. The difference of the OH production in the early morning hours can be seen easily. After 1200 GMT (20 July) and 0800 GMT (21 July), $J(HCHO_{rad})$ has been modeled because no measurements were available for this time period. The dotted line shows the calculated OH from the photolysis of the HONO formed during daytime.

[52] This OH production mechanism is independent of solar radiation. It therefore proceeded throughout the day. At night it was the most important OH formation mechanism producing about 10^6 OH cm^{-3} s^{-1} on 21 July at night. During the day, with lower terpene concentrations, the formation was lower. With the exception of NO_3 + VOC this was the only source of hydroxyl radicals during the night [see *Geyer et al.*, 2001, 2003].

3.5.5. Reaction of NO_3 With Monoterpenes

[53] Hydroxyl radicals can also be formed by the reaction of the nitrate radical with alkenes. The importance of this mechanism was modeled by *Geyer et al.* [2003] and

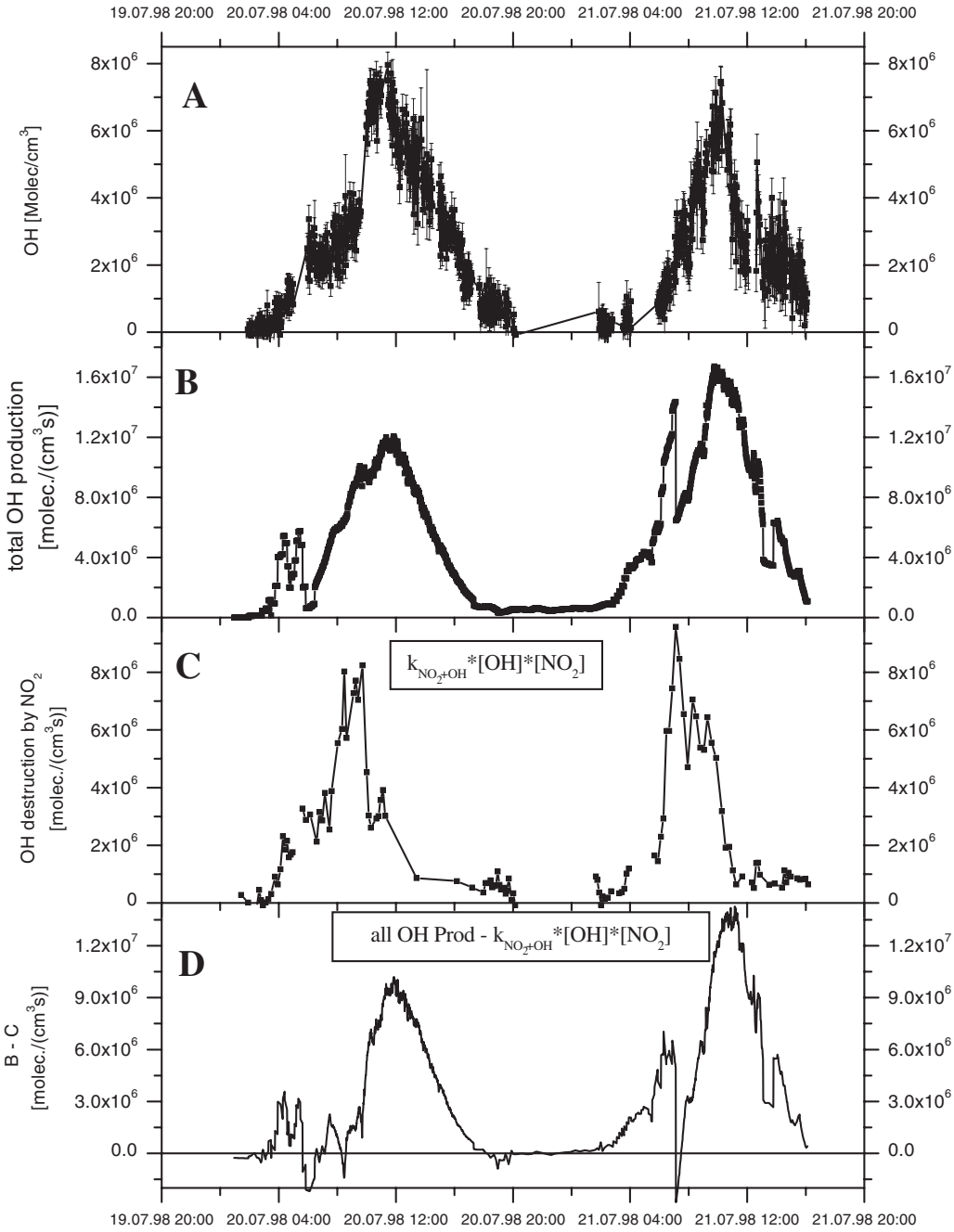

Figure 12. Net OH production during 19–21 July 1998 at Pabstthum. Graphs A and B present the measured OH concentrations and the total calculated OH production. Assuming that the main OH loss mechanism in the morning is its reaction with NO_2, the OH loss can be calculated from the OH and NO_2 concentration (graph C). The subtraction of graphs B and C yields the net OH production (graph D). The OH formation by HONO photolysis is responsible for starting the photochemistry in the early morning.

represented an additional OH source during the night of about 25% compared to the ozone + alkene reaction. Integrated over 24 hours, this source contributed to less than 2% of the total OH production mechanisms.

3.6. Comparison of the Contribution of the Different OH Production Mechanisms

[54] Figure 11 summarizes and compares the different OH formation mechanisms discussed above. Before sunrise only the reactions of ozone with alkenes and the reaction of NO with RO_2 from NO_3 reactions produce OH radicals. This changes at sunrise when, for about 3–4 hours, HONO photolysis is by far the most important source, with peak formation rates of $(5.3 \pm 1.1) \times 10^6$ and $(8.0 \pm 2.1) \times 10^6$ cm^{-3} s^{-1} on 20 and 21 July, respectively. The only other nonnegligible process at this time of the day was the reaction of ozone with alkenes, which produced up to $(1.8 \pm 0.7) \times 10^6$ cm^{-3} s^{-1} at 0323 GMT on 21 July. As

discussed above, the HCHO photolysis becomes important only after most of the nighttime HONO has been photolyzed, around 7–8 GMT. Considering the error in our HCHO measurements, the formaldehyde photolysis constitutes an OH source comparable in magnitude to ozone photolysis. Both pathways follow solar radiation, showing a maximum around noon. The peak formation rates for both processes are in the range of 6×10^6 cm^{-3} s^{-1}. During the day the HONO photolysis and O_3 + alkene reactions only play a minor role compared to the much stronger ozone and HCHO photolysis pathways.

[55] To estimate the role of the different pathways for the total OH production over the day we integrated the OH yielding processes (see Figure 11 and Table 4) over 24 hours. The highest value is provided by the O_3 photolysis (reaction (2)) with 6.0 ± 0.7 ppb (5.2 ± 0.6 ppb for 21 July) of OH during 24 hours. The photolysis of formaldehyde (reaction (5) + (7) − (9)) plays a major role at the Pabstthum site, as previously postulated by *Ehhalt et al.* [1998] and *Kleinman et al.* [1995]. The OH production integrated over a 24 hour period is 4.6 ± 0.9 ppb (6.4 ± 1.2 ppb for 21 July).

[56] As noted above, the formaldehyde measurements carried out at a height of 8 m with the Hantzsch monitor show about two times smaller values. Calculating with these concentrations, the maximum of OH produced by HCHO is 3.2 ± 0.5 ppb for 20 July and 4.4 ± 0.7 ppb of OH production on 21 July. By these values, the importance of HONO for the total OH budget even becomes more significant.

3.7. Comparison With OH and HO_2 Measurements

[57] On a first view the direct comparison of the calculated OH production rate by HONO photolysis with measured OH concentrations [*Holland et al.*, 2003] at the BERLIOZ site Pabstthum gives no direct evidence for the additional OH source by photolysis of HONO (Figure 12). Note, however, that there is a gap in the morning OH measurement data during the highest peak of OH production from J(HONO) on 20 July and for a few hours on 21 July 1998 as well. Nevertheless there is some evidence for the role of HONO photolysis for OH production: The OH levels start to increase around 0400 GMT while its earliest increase is expected at 0600 GMT from pure ozone photolysis. At 0500 GMT the OH concentration surpasses 10^6 cm^{-3} (Figure 12). Although the OH production at 0500 GMT is similar to noon values, the OH concentration of $\approx 10^6$ cm^{-3} is clearly below the noon level.

[58] It was recently suggested that the HONO production of OH in the morning is absorbed by the elevated NO_2 concentrations that are simultaneously present. The OH formed by HONO photolysis can react with NO_2 and form HNO_3:

$$OH + NO_2 \rightarrow HNO_3 \qquad (20)$$

[59] To calculate the production of OH radicals available to the oxidation of hydrocarbons we subtracted the rate of OH destruction by reaction (20) from the total OH formation by all mechanisms described above. Figure 12 shows that, particularly in the late morning hours when the NO_2 concentration is still high, the destruction of OH by NO_2 is important. Nevertheless we found a positive OH production on both days, mainly by HONO photolysis in the early morning (see Figure 12D). Only later in the morning an overall net OH destruction is observed for about 1–2 hours. We therefore conclude that HONO photolysis represents an OH source in the early morning hours, which starts the ozone production by oxidizing hydrocarbons.

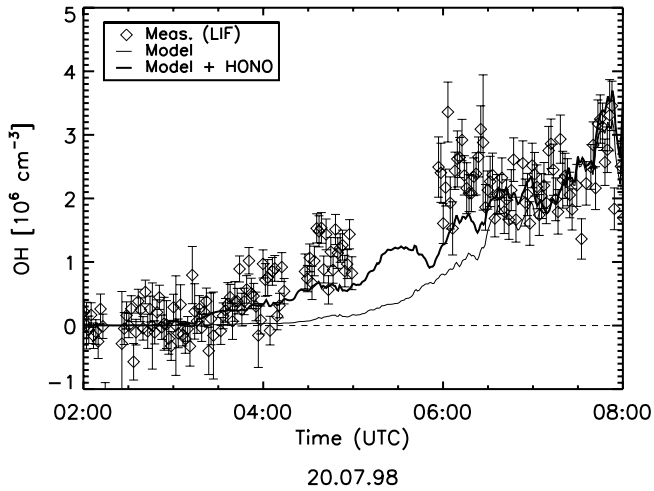

Figure 13. Comparison of the modeled OH concentrations in the early morning of 20 July 1998 at the BERLIOZ site Pabstthum including the photolysis of HONO (thick line) and without (thin line).

[60] A first attempt to compare the measured OH data in the morning with modeled OH concentrations was made using a box model with a CO–CH_4–NO_x chemistry module including acetaldehyde and PAN. Other VOCs were neglected. This model was successfully tested in the past on the POPCORN data set [*Ehhalt*, 1999]. (The model overestimated the OH measurements on average by 10%.)

[61] Without including the photolysis of HONO in the model, the OH concentration is underestimated by a factor of about 10 at 0430 GMT in the morning (see Figure 13). This large disagreement could only be removed by including the photolysis of HONO into the model [see *Platt et al.*, 2002]. Since the OH production via this process is driven by longer-wavelength radiation than the ozone photolysis OH concentrations start to rise earlier in the morning than predicted by ozone photolysis alone. A model for the complete OH chemistry will be employed in the future to investigate the influence of HONO on ozone formation in more detail.

4. Conclusion

[62] A comparison of the different OH formation mechanisms that were determined from measurements during the 1998 BERLIOZ field campaign at Pabstthum shows the importance of the individual processes at different times of day. While ozone and HCHO photolysis are the most important OH-forming mechanisms during most of the day, the data clearly shows the high importance of HONO in the early morning hours. The peak OH formation rate by

HONO photolysis is comparable to the one by ozone photolysis at noon, but the formation only lasts for about 3–4 hours. Although HONO is only found in the presence of elevated NO_2 concentrations, which can remove the OH via the formation of HNO_3, we found a net OH production rate available for VOC oxidation from HONO photolysis. This shows that HONO photolysis can indeed start and accelerate the oxidation processes in the morning.

[63] The integrated morning OH formation of 1.0 ± 0.2 ppb (1.8 ± 0.3 ppb for 21 July) from HONO photolysis has to be compared to the 24h integrals of the other OH sources ($J(HCHO_{rad})$ + $J(O^1D)$ + OH from the VOCs) which form together 11.4 ± 1.9 ppb of OH (13.4 ± 2.5 ppb for 21 July). The morning HONO peak alone constitutes around 10–15% of the total daily OH formation. Calculating the HONO source strength from the increase of HONO during the night, we get an additional OH production during daytime of 0.8±0.4 ppb (1.4 ± 0.5 ppb for 21 July) for the measured photolysis frequencies and NO_2 concentrations on the example day 20 July 1998. The integrated OH production over 24 hours shows that the photolysis of HONO contributed up to 20% of the total hydroxyl radical amount during these days at Pabstthum.

[64] **Acknowledgments.** This project was supported by the BMBF in the framework of TFS-LT3 (contract 422-4007-07TFS 31/H.B.3). We would like to thank two anonymous referees for their careful revision of the manuscript and their helpful comments to improve the paper.

References

Alicke, B., U. Platt, and J. Stutz, Impact of nitrous acid photolysis on the total hydroxyl radical budget during the Limitation of Oxidant Production/Pianura Padana Produzione di Ozono study in Milan, *J. Geophys. Res.*, *107*(D22), 8196, doi:10.1029/2000JD000075, 2002.

Allegrini, I., and A. Febo, Role of nitrous acid on the oxidation processes in the Mediterranean urban areas, *Ann. Chim.*, *85*(7–8), 471–485, 1995.

Ammann, M., M. Kalberer, D. T. Jost, L. Tobler, E. Rossler, D. Piguet, H. W. Gaggeler, and U. Baltensperger, Heterogeneous production of nitrous acid on soot in polluted air masses, *Nature*, *395*, 157–160, 1998.

Atkinson, R., Gas-phase tropospheric chemistry of volatile organic compounds, 1, Alkanes and alkenes, *J. Phys. Chem. Ref. Data*, *26*, 215–290, 1997.

Atkinson, R., and S. M. Aschmann, OH radical production from the gas-phase reactions of O_3 with a series of alkenes under atmospheric conditions, *Environ. Sci. Technol.*, *27*, 1357–1363, 1993.

Bey, I., G. Aumont, and G. Toupance, A modelling study of the nighttime radical chemistry in the lower continental troposphere, 2, Origin and evolution of HO_x, *J. Geophys. Res.*, *106*, 9991–10001, 2001.

Brauers, T., M. Hausmann, U. Brandenburger, and H. P. Dorn, Improvement of differential optical absorption spectroscopy with a multichannel scanning technique, *Appl. Opt.*, *34*(21), 4472–4479, 1995.

Brauers, T., U. Aschmutat, U. Brandenburger, H. P. Dorn, M. Hausmann, M. Hessling, A. Hofzumahaus, F. Holland, C. Plassdulmer, and D. H. Ehhalt, Intercomparison of tropospheric OH radical measurements by multiple folded long-path laser absorption and laser induced fluorescence, *Geophys. Res. Lett.*, *23*, 2545–2548, 1996.

Calvert, J. G., G. Yarwood, and A. M. Dunker, An evaluation of the mechanism of nitrous acid formation in the urban atmosphere, *Res. Chem. Intermed.*, *20*(3–5), 463–502, 1994.

Chan, W. H., R. J. Nordstrom, J. G. Calvert, and J. H. Shaw, Kinetic study of HONO formation and decay reactions in gaseous mixtures of HONO, NO, NO_2, H_2O, and N_2, *Environ. Sci. Technol.*, *10*, 674–682, 1976.

Criegee, R., Mechanisms of ozonolysis, *Angew. Chem. Int. Ed. Engl.*, *14*, 745–752, 1975.

Crutzen, P. J., and P. H. Zimmermann, The changing photochemistry of the troposphere, *Tellus*, *43*, 136–151, 1991.

Ehhalt, D. H., Photooxidation of trace gases in the troposphere, *Phys. Chem. Chem. Phys.*, *1*, 5401–5408, 1999.

Ehhalt, D. H., F. Rohrer, A. Wahner, M. J. Prather, and D. R. Blake, On the use of hydrocarbons for the determination of tropospheric OH concentrations, *J. Geophys. Res.*, *103*, 18,981–18,997, 1998.

Eisele, F. L., G. H. Mount, D. Tanner, A. Jefferson, R. Shetter, J. W. Harder, and E. J. Williams, Understanding the production and interconversion of the hydroxyl radical during the Tropospheric OH Photochemistry Experiment, *J. Geophys. Res.*, *102*, 6457–6465, 1997.

Febo, A., C. Perrino, and I. Allegrini, Measurement of nitrous acid in Milan, Italy, by DOAS and diffusion denuders, *Atmos. Environ.*, *30*, 3599–3609, 1996.

Febo, A., C. Perrino, and M. Cortiello, A denuder technique for the measurement of nitrous acid in urban atmospheres, *Atmos. Environ.*, *27*, 1721–1728, 1993.

Finlayson-Pitts, B. J. and J. N. Pitts, *Chemistry of the Upper and Lower Atmosphere: Theory, Experiments and Applications*, xxii, 969 pp., Academic, San Diego, Calif., 2000.

Geyer, A., B. Alicke, D. Mihelcic, J. Stutz, and U. Platt, Comparison of tropospheric NO_3 radical measurements by differential optical absorption spectroscopy and matrix isolation electron spin resonance, *J. Geophys. Res.*, *104*, 26,097–26,105, 1999.

Geyer, A., B. Alicke, S. Konrad, T. Schmitz, J. Stutz, and U. Platt, Chemistry and oxidation capacity of the nitrate radical in the continental boundary layer near Berlin, *J. Geophys. Res.*, *106*, 8013–8025, 2001.

Geyer, A., et al., Nighttime formation of peroxy and hydoxyl radicals during the BERLIOZ campaign: Observations and modeling studies, *J. Geophys. Res.*, *108*, doi:10.1029/2001JD000656, in press, 2003.

Goodman, A. L., G. M. Underwood, and V. H. Grassian, Heterogeneous reaction of NO_2: Characterization of gas-phase and adsorbed products from the reaction, 2 $NO_2(g)$ + $H_2O(a)$ → $HONO(g)$ + $NO_3(a)$ on hydrated silica particles, *J. Phys. Chem. A*, *103*, 7217–7223, 1999.

Grossmann, D., G. Moortgat, M. Kibler, S. Schlomski, K. Bachmann, B. Alicke, A. Geyer, U. Platt, M. Hammer, and B. Vogel, Hydrogen peroxide, organic peroxides, carbonyl compounds and organic acids measured in Pabstthum during BERLIOZ, *J. Geophys. Res.*, *108*, doi:10.1029/2001JD001096, in press, 2003.

Harder, J. W., J. W. Brault, P. V. Johnston, and G. H. Mount, Temperature dependent NO_2 cross section at high spectral resolution, *J. Geophys. Res.*, *102*, 3861–3879, 1997.

Harris, G. W., W. P. L. Carter, A. M. Winer, J. N. Pitts, U. Platt, and D. Perner, Observations of nitrous acid in the Los Angeles atmosphere and implications for the predictions of ozone–precursor relationships, *Environ. Sci. Technol.*, *16*, 414–419, 1982.

Harrison, R. M., and A. M. N. Kitto, Evidence for a surface source of atmospheric nitrous acid, *Atmos. Environ.*, *28*, 1089–1094, 1994.

Harrison, R. M., J. D. Peak, and G. M. Collins, Tropospheric cycle of nitrous acid, *J. Geophys. Res.*, *101*, 14,429–14,439, 1996.

Hofzumahaus, A., A. Kraus, and M. Muller, Solar actinic flux spectroradiometry: A technique for measuring photolysis frequencies in the atmosphere, *Appl. Opt.*, *38*(21), 4443–4460, 1999.

Holland, F., U. Aschmutat, M. Hessling, A. Hofzumahaus, and D. H. Ehhalt, Highly time resolved measurements of OH during POPCORN using laser-induced fluorescence spectroscopy, *J. Atmos. Chem.*, *31*, 205–225, 1998.

Holland, F., A. Hofzumahaus, J. Schäfer, A. Kraus, and H.-W. Patz, Measurements of OH and H_2O radical concentrations and photolysis frequencies during BERLIOZ, *J. Geophys. Res.*, *108*, doi:10.1029/2001JD001393, in press, 2003.

Howard, C. J., Kinetics of the reaction of HO_2 with NO_2, *J. Chem. Phys.*, *67*, 5258–5263, 1977.

Jenkin, M. I., R. A. Cox, and D. J. Williams, Laboratory studies of the kinetics of formation of nitrous acid from the thermal reaction of nitrogen dioxide and water vapour, *Atmos. Environ.*, *22*, 487–498, 1988.

Junkermann, W., and T. Ibusuki, FTIR spectroscopic measurements of surface bond products of nitrogen oxides on aerosol surfaces: Implications for heterogeneous HNO_2 production, *Atmos. Environ.*, *26*, 3099–3103, 1992.

Kaiser, E. W., and C. H. Wu, Measurement of the rate constant of the reaction of nitrous acid with nitric acid, *J. Phys. Chem.*, *81*, 187–190, 1977.

Kalberer, M., M. Ammann, F. Arens, H. W. Gaggeler, and U. Baltensperger, Heterogeneous formation of nitrous acid (HONO) on soot aerosol particles, *J. Geophys. Res.*, *104*, 13,825–13,832, 1999.

Kessler, C. and U. Platt, Nitrous acid in polluted air masses: Sources and formation pathways, *Proceeding on the 3rd Eur. Symp. on Phys. Chem. Behav. of Atmos. Pollut., Varese, Italia, 10–12 Apr.*, pp. 412–422, D. Reidell, Norwell, Mass., 1984.

Kleinman, L., L. Yin-Nan, S. R. Springston, J. H. Lee, L. Nunnermacker, J. Weinstein-Lloyd, Z. Xianliang, and L. Newman, Peroxy radical concentration and ozone formation rate at a rural site in the southeastern United States, *J. Geophys. Res.*, *100*, 7263–7273, 1995.

Knoll, P., R. Singer, and W. Kiefer, Improving spectroscopic techniques by a scanning multichannel method, *Appl. Spectrosc.*, *44*, 776–782, 1990.

Konrad, S., and A. Volz-Thomas, Characterization of a commercial gas chromatography–flame ionization detection system for the in situ deter-

mination of C5–C10 hydrocarbons in ambient air, *J. Chromatogr. A*, *872*(2), 215–234, 2001.
Kraus, A., and A. Hofzumahaus, Field measurements of atmospheric photolysis frequencies for O_3, NO_2, HCHO, CH_3CHO, H_2O_2, and HONO by UV spectroradiometry, *J. Atmos. Chem.*, *31*, 161–180, 1998.
Lammel, G., and J. N. Cape, Nitrous acid and nitrite in the atmosphere, *Chem. Soc. Rev.*, *25*(5), 361, 1996.
Lammel, G., and D. Perner, The atmospheric aerosol as a source of nitrous acid in the polluted atmosphere, *J. Aerosol Sci.*, *19*, 1199–1202, 1988.
Logan, J. I., M. J. Prather, S. C. Wofsy, and M. B. McElroy, Tropospheric chemistry: A global perspective, *J. Geophys. Res.*, *86*, 7210–7254, 1981.
Longfellow, C. A., T. Imamura, A. R. Ravishankara, and D. R. Hanson, HONO solubility and heterogeneous reactivity on sulfuric acid surfaces, *J. Phys. Chem. A*, *102*, 3323–3332, 1998.
Meller, R., and G. K. Moortgart, Temperature dependence of the absorption cross sections of formaldehyde between 223 and 323 K in the wavelength range 225–375 nm, *J. Geophys. Res.*, *201*, 7089–7101, 2000.
Mihelcic, D., F. Holland, A. Hofzumahaus, L. Hoppe, S. Konrad, P. Müsgen, H.-W. Pätz, H.-J. Schäfer, T. Schmitz, and A. Volz-Thomas, Peroxy radicals during BERLIOZ at Pabstthum: Measurements, radical, budgets, and ozone production,, *J. Geophys. Res.*, *108*, doi:10.1029/2001JD001014, in press, 2003.
Müller, M., A. Kraus, and A. Hofzumahaus, O-3-P O(D-1) Photolysis frequencies determined from spectroradiometric measurements of solar actinic UV-radiation: Comparison with chemical actinometer measurements, *Geophys. Res. Lett.*, *22*, 679–682, 1995.
Nguyen, M. T., R. Sumathi, D. Sengupta, and J. Peeters, Theoretical analysis of reactions related to the HNO_2 energy surface: OH + NO and H + NO_2, *Chem. Phys.*, *230*(1), 1–11, 1998.
Notholt, J., J. Hjorth, and F. Raes, Formation of HNO_2 on aerosol surfaces during foggy periods in the presence of NO and NO_2, *Atmos. Environ.*, *26A*, 211–217, 1992.
Paulson, S. E., A. D. Sen, L. Ping, J. D. Fenske, and M. J. Fox, Evidence for formation of OH radicals from the reaction of O_3 with alkenes in the gas phase, *Geophys. Res. Lett.*, *24*, 3193–3196, 1997.
Paulson, S. E., M. Y. Chung, and A. S. Hasson, OH radical formation from the gas-phase reaction of ozone with terminal alkenes and the relationship between structure and mechanism, *J. Phys. Chem. A*, *103*, 8125–8138, 1999.
Perner, D., and U. Platt, Detection of nitrous acid in the atmosphere by differential optical absorption, *Geophys. Res. Lett.*, *6*, 917–920, 1979.
Pitts, J. N., E. Sanhueza, R. Atkinson, W. P. L. Carter, A. M. Winer, G. W. Harris, and C. N. Plum, An investigation of the dark formation of nitrous acid in environmental chambers, *Int. J. Chem. Kinet.*, *XVI*, 919–939, 1984.
Platt, U., *The Origin of Nitrous and Nitric Acid in the Atmosphere*, edited by W. Jaeschke, pp. 299–319, Springer-Verlag, New York, 1986.
Platt, U., Differential Optical Absorption Spectroscopy (DOAS), in *Monitoring by Spectroscopic Techniques*, edited by M. W. Sigrist, pp. 27–84, John Wiley, New York, 1994.
Platt, U., and D. Perner, Direct measurements of atmospheric CH_2O, HNO_2, O_3, NO_2, and SO_2 by differential optical absorption in the near UV, *J. Geophys. Res.*, *85*, 7453–7458, 1980.
Platt, U., D. Perner, G. W. Harris, A. M. Winer, and J. N. Pitts, Observations of nitrous acid in an urban atmosphere by differential optical absorption, *Nature*, *285*, 312–314, 1980.
Platt, U., G. Lebras, G. Poulet, J. P. Burrows, and G. Moortgat, Peroxy radicals from night-time reaction of NO_3 with organic compounds, *Nature*, *348*, 147–149, 1990.
Platt, U., et al., Free radicals and fast photochemistry during BERLIOZ, *J. Atmos. Chem.*, *42*, 359–394, 2002.
Prinn, R. G., R. F. Weiss, B. R. Miller, J. Huang, F. N. Alyea, D. M. Cunnold, P. J. Fraser, D. E. Hartley, and P. G. Simmonds, Atmospheric trends and lifetime of CH_3CCl_2 and global OH concentrations, *Science*, *269*(5221), 187–192, 1995.
Ritz, D., M. Hausmann, and U. Platt, An improved open multi-path reflection cell for the measurement of NO_2 and NO_3, in *Optical Methods in Atmospheric Chemistry*, edited by H. Schiff and U. Platt, *Proc. SPIE Int. Soc. Opt. Eng. 1715*, 200–211, 1992.
Ruggaber, A., R. Dlugi, and T. Nakajima, Modelling radiation quantities and photolysis frequencies in the troposphere, *J. Atmos. Chem.*, *18*, 171–210, 1994.
Sakamaki, F., S. Hatakeyama, and H. Akimoto, Formation of nitrous acid and nitric oxide in the heterogeneous dark reaction of nitrogen dioxide and water vapor in a smog chamber, *Int. J. Chem. Kinet.*, *XV*, 1013–1029, 1983.
Schneider, W., G. K. Moortgat, G. S. Tyndall, and J. P. Burrows, Absorption cross-sections of NO_2 in the UV and visible region (200–700 nm) at 298 K, *J. Photochem. Photobiol.*, *40*, 195–217, 1987.
Sjödin, A., Studies of the diurnal variation of nitrous acid in urban air, *Environ. Sci. Technol.*, *22*, 1086–1089, 1988.
Sjödin, A., and M. Ferm, Measurement of nitrous acid in an urban area, *Atmos. Environ.*, *19*, 985–992, 1985.
Stockwell, R. W., and J. G. Calvert, The near ultraviolet absorption spectrum of gaseous HONO and N_2O_3, *J. Photochem.*, *8*, 193–203, 1978.
Stuhl, F., and H. Niki, Flash photochemical study of the reaction OH + NO + M using resonance fluorescent detection of OH, *J. Chem. Phys.*, *57*, 3677–3679, 1972.
Stutz, J., Messung der Konzentration troposphärischer Spurenstoffe mittels Differentieller Optischer Absorptionspektroskopie: Eine neue Gerneration von Geräten und Algorithmen, Ph.D. thesis, Univ. Heidelberg, Heidelberg, 1996.
Stutz, J., and U. Platt, Problems in using diode arrays for open path DOAS measurements of atmospheric species, in *Optical Methods in the Atmospheric Chemistry*, *Proc. SPIE Int. Soc. Opt. Eng. 1715*, 329–340, 1992.
Stutz, J., and U. Platt, Numerical analysis and estimation of the statistical error of differential optical absorption spectroscopy measurements with least-squares methods, *Appl. Opt.*, *35*(30), 6041–6053, 1996.
Stutz, J., and U. Platt, Improving long-path differential optical absorption spectroscopy with a quartz-fiber mode mixer, *Appl. Opt.*, *36*(6), 1105–1115, 1997.
Stutz, J., E. S. Kim, U. Platt, P. Bruno, C. Perrino, and A. Febo, UV-visible absorption cross section of nitrous acid, *J. Geophys. Res.*, *105*, 14,585–14,592, 2000.
Stutz, J., B. Alicke, and A. Neftel, Nitrous acid formation in the urban atmosphere: Gradient measurements of NO_2 and HONO over grass in Milan, Italy, *J. Geophys. Res.*, *107*(D22), 8192, doi:10.1029/2001JD000390, 2002.
Svensson, R., E. Ljungström, and O. Lindqvist, Kinetics of the reaction between nitrogen dioxide and water vapour, *Atmos. Environ.*, *21*, 1529–1539, 1987.
Tyndall, G. S., J. J. Orlando, and J. G. Calvert, Upper limit for the rate coefficient for the reaction $HO_2 + NO_2 \rightarrow HONO + O_2$, *Environ. Sci. Technol.*, *29*, 202–206, 1995.
Veitel, H., Vertical profiles of NO_2 and HONO in the planetary boundary layer, Ph.D. thesis, Univ. Heidelberg, Heidelberg, Germany, 2002.
Volz-Thomas, A., H. Geiss, A. Hofzumahaus, and K.-H. Becker, Fast photochemistry experiment in BERLIOZ (PHOEBE): An introduction, *J. Geophys. Res.*, *108*, doi:10.1029/2001JD002029 in press, 2003a.
Volz-Thomas, A., H.-W. Patz, N. Houben, S. Konrad, D. Mihelcic, T. Klupfel, and D. Perner, Inorganic trace gases and peroxy radicals during BERLIOZ at Pabstthum: An investigation of the photostationary state of NO_x and O_3, *J. Geophys. Res.*, *108*, doi:10.1029/2001JD001255 in press, 2003b.
White, J. U., Long optical paths of large aperture, *J. Opt. Soc. Am.*, *32*, 285–288, 1942.
White, J. U., Very long optical paths in air, *J. Opt. Soc. Am.*, *66*, 411–416, 1976.
Winer, A. M., and H. W. Biermann, Long pathlength Differential Optical Absorption Spectroscopy (DOAS) measurements of gaseous HONO, NO_2 and HCHO in the California South Coast Air Basin, *Res. Chem. Intermed.*, *20*(3–5), 423–445, 1994.

B. Alicke and U. Platt, Institut für Umweltphysik, Universitat Heidelberg, INF 229, D-69120 Heidelberg, Germany. (Andreas.Geyer@iup.uni-heidelberg.de)

A. Hofzumahaus, F. Holland, S. Konrad, H. W. Pätz, J. Schäfer, and A. Volz-Thomas, Stettiner Staatsforst, Forschungszentrum Jülich, D-52425 Jülich, Germany.

J. Stutz and A. Geyer, Department of Atmospheric Sciences, University of California, Los Angeles, 7172 Math Sciences, Box 951565, Los Angeles, CA 90095-1565, USA.